iPSCs can be differentiated into the affected cell types or tissues, allowing direct functional assays to be performed that are associated with the pathology. Second, because the disease-causing potential of some mutations is dependent on the genetic backgrounds of the patients,[38] it may be better to obtain both mutant and wild-type clones from a single mosaic patient to more accurately assess the impact of the mutation(s).

Considering that a mutation of *NLRP3* in 10% of the cells is sufficient to cause a distinct disease phenotype, somatic mutations of various genes at an even rarer frequency may also affect the biologic characteristics of a person. Because the presence of the *NLRP3* mutation did not affect the efficacy of reprogramming to the iPSCs, we may be able to obtain both mutant and wild-type iPSC clones from CINCA syndrome patients who carry *NLRP3* mutant cells at a lower percentage. In some diseases, such as Fanconi anemia, however, mutant cells may be resistant to reprogramming.[39,40] Even though there are some possible limitations, establishing both mutant and wild-type iPSC clones is a promising approach to dissect the extent and role of somatic mosaicism.

We demonstrated that several inhibitors that are considered to be effective against CINCA syndrome actually attenuated the disease-relevant phenotype of iPSC-derived macrophages. Before a successful drug screening using iPSC-derived somatic cells can be developed, several limitations need to be overcome, such as the heterogeneity of differentiation and difficulties associated with purification.[18] In this report, we used an efficient and robust differentiation protocol and obtained plenty of macrophages free from the clonal variations.

In conclusion, we elucidated the pathologic roles of both mutant and wild-type cells in mosaic CINCA syndrome patients. After obtaining iPSC-derived macrophages in large quantity and with high purity, we showed they are applicable for drug screening. The iPSC-based approach may help to illuminate the pathogenesis of various diseases that are caused by somatic mosaicism, and facilitate drug discovery for the treatment of NLRP3-related inflammatory diseases.

Acknowledgments

The authors thank the CINCA syndrome patients who participated in this study; Y. Sasaki, Y. Jindai, A. Okada, M. Narita, A. Nagahashi, T. Ohkame, S. Nishimoto, Y. Inoue, and S. Arai for technical assistance; I. Kato for help with animal experiments; M. Nakagawa, K. Okita, Y. Yoshida, T. Aoi, and M. Yanagimachi for scientific comments; and R. Kato, E. Nishikawa, S. Takeshima, Y. Otsu, H. Hasaba, H. Watanabe, T. Ishii, H. Kurokawa, N. Takasu, and Y. Takao for administrative assistance.

This work was supported by the Ministry of Health, Labor and Welfare (N.M. and T.N.), the Ministry of Education, Culture, Sports, Science and Technology (MEXT; N.M. and T.N.), the Leading Project of MEXT (S.Y. and T.N.), the Promotion of Fundamental Studies in Health Sciences of National Institute of Biomedical Innovation (S.Y.), the Funding Program for World-Leading Innovative Research and Development on Science and Technology (FIRST Program) of Japan Society for the Promotion of Science (JSPS; T.N., and S.Y.), JSPS and MEXT (Grants-in-Aid for Scientific Research; S.Y.), JSPS (T.N., T.T., and M.K.S.), the Takeda Science Foundation, SENSHIN Medical Research Foundation, and Suzuken Memorial Foundation to (M.K.S.).

Authorship

Contribution: T.T. planned the project, established iPSCs, performed experimental work, analyzed data, and prepared the manuscript; K.T. planned the project, established iPSCs, and analyzed data; M.Y., S.T., and S.N. performed experimental work; K.O., A.N., and T.H. analyzed data; R.N. and N.K. planned the project; H.H. and M.M. performed *L monocytogenes* infection; N.M. and J.E.H. performed electron microscopy; T.Y. identified retroviral integration sites; A.W. performed bisulfite sequencing; A.S.-O. and S.O. analyzed CNV; I.A. established iPSCs; S.Y. and T.N. planned the project and analyzed data; M.K.S. planned the project, analyzed data, and prepared the manuscript; and all authors read and approved the manuscript.

Conflict-of-interest disclosure: S.Y. is a member without salary of the scientific advisory boards of iPierian, iPS Academia Japan, and Megakaryon Corporation. The remaining authors declare no competing financial interests.

Correspondence: Megumu K. Saito, Center for iPS Cell Research and Application, Kyoto University, Kyoto 606-8507, Japan; e-mail: msaito@cira.kyoto-u.ac.jp.

References

1. Prieur AM riscelli C Lampert F et al. A chronic in antile neurolo ical cutaneous and articular (CINCA) syndrome a speci c entity analysed in 30 patients. *Scand J Rheumatol Suppl.* 1987 66 57-68.
2. A senti evich I Nowa M Mallah M et al. De novo CIAS1 mutations cyto ine activation and evidence or enetic hetero eneity in patients with neonatal-onset multisystem in ammatory disease (N MID) a new member o the e pandin amily o pyrin-associated autoin ammatory diseases. *Arthritis Rheum.* 2002 46(12) 3340-3348.
3. Feldmann Prieur AM uartier P et al. Chronic in antile neurolo ical cutaneous and articular syndrome is caused by mutations in CIAS1 a ene hi hly e pressed in polymorphonuclear cells and chondrocytes. *Am J Hum Genet.* 2002 71(1) 198-203.
4. Bauern eind F Horvath Stut A et al. Cuttin ed e NF- appaB activatin pattern reco nition and cyto ine receptors license NLRP3 in ammasome activation by re ulatin NLRP3 e pression. *J Immunol.* 2009 183(2) 787-791.
5. Mariathasan S Weiss DS Newton et al. Cryopyrin activates the in ammasome in response to to ins and ATP. *Nature.* 2006 440(7081) 228-232.
6. attorno M Tassi S Carta S et al. Pattern o interleu in-1beta secretion in response to lipopolysaccharide and ATP be ore and a ter interleu in-1 bloc ade in patients with CIAS1 mutations. *Arthritis Rheum.* 2007 56(9) 3138-3148.
7. oldbach-Mans y R Dailey N Canna SW et al. Neonatal-onset multisystem in ammatory disease responsive to interleu in-1beta inhibition. *N Engl J Med.* 2006 355(6) 581-592.
8. Neven B Marvillet I Terrada C et al. Lon -term e cacy o the interleu in-1 receptor anta onist ana inra in ten patients with neonatal-onset multisystem in ammatory disease/chronic in antile neurolo ic cutaneous articular syndrome. *Arthritis Rheum.* 2010 62(1) 258-267.
9. Saito M Nishi omori R ambe N et al. Disease-associated CIAS1 mutations induce monocyte death revealin low-level mosaicism in mutationne ative cryopyrin-associated periodic syndrome patients. *Blood.* 2008 111(4) 2132-2141.
10. Tana a N I awa Saito M et al. Hi h incidence o NLRP3 somatic mosaicism in patients with chronic in antile neurolo ic cutaneous articular syndrome results o an International Multicenter Collaborative Study. *Arthritis Rheum.* 2011 63(11) 3625-3632.
11. Masters SL Simon A A senti evich I astner DL. Horror autoin ammaticus the molecular pathophysiolo y o autoin ammatory disease. *Annu Rev Immunol.* 2009 27 621-668.
12. oussou an H Pyerit R . Mechanisms and conse uences o somatic mosaicism in humans. *Nat Rev Genet.* 2002 3(10) 748-758.
13. ric son RP. Somatic ene mutation and human disease other than cancer an update. *Mutat Res.* 2010 705(2) 96-106.
14. Ari a T ondoh T ama uchi et al. Spontaneous in vivo reversion o an inherited mutation in the Wis ott-Aldrich syndrome. *J Immunol.* 2001 166(8) 5245-5249.

15. Nishi omori R A uta awa H Maruyama et al. -lin ed ectodermal dysplasia and immunode - ciency caused by reversion mosaicism o N M reveals a critical role or N M in human T-cell development and/or survival. *Blood.* 2004 103(12) 4565-4572.
16. Luts iy MI Beardsley DS Rosen FS Remold- Donnell . Mosaicism o N cells in a patient with Wis ott-Aldrich syndrome. *Blood.* 2005 106(8) 2815-2817.
17. Ta ahashi Tanabe hnu i M et al. Induction o pluripotent stem cells rom adult human broblasts by de ned actors. *Cell.* 2007 131(5) 861-872.
18. rs ovic M avaherian A Strulovici B Daley . Induced pluripotent stem cells opportunities or disease modellin and dru discovery. *Nat Rev Drug Discov.* 2011 10(12) 915-929.
19. Hanna Mar oula i S Schorderet P et al. Direct repro rammin o terminally di erentiated mature B lymphocytes to pluripotency. *Cell.* 2008 133(2) 250-264.
20. Saito M Fu isawa A Nishi omori R et al. Somatic mosaicism o CIAS1 in a patient with chronic in antile neurolo ic cutaneous articular syndrome. *Arthritis Rheum.* 2005 52(11) 3579-3585.
21. Na ano T odama H Hon o T. eneration o lymphohematopoietic cells rom embryonic stem cells in culture. *Science.* 1994 265(5175) 1098-1101.
22. Fu isawa A ambe N Saito M et al. Disease-associated mutations in CIAS1 induce cathepsin B-dependent rapid cell death o human THP-1 monocytic cells. *Blood.* 2007 109(7) 2903-2911.
23. Willin ham SB Ber stralh DT Connor W et al. Microbial patho en-induced necrotic cell death mediated by the in ammasome components CIAS1/cryopyrin/NLRP3 and ASC. *Cell Host Microbe.* 2007 2(3) 147-159.
24. Iyer SS Puls ens WP Sadler et al. Necrotic cells tri er a sterile in ammatory response throu h the Nlrp3 in ammasome. *Proc Natl Acad Sci U S A.* 2009 106(48) 20388-20393.
25. Bei i RD ertesy SB A uilina Dubya R. idi ed ATP (oATP) attenuates proin ammatory si nalin via P2 receptor-independent mechanisms. *Br J Pharmacol.* 2003 140(3) 507-519.
26. Martinon F Petrilli V Mayor A Tardivel A Tschopp . out-associated uric acid crystals activate the NALP3 in ammasome. *Nature.* 2006 440(7081) 237-241.
27. Halle A Hornun V Pet old C et al. The NALP3 in ammasome is involved in the innate immune response to amyloid-beta. *Nat Immunol.* 2008 9(8) 857-865.
28. Duewell P ono H Rayner et al. NLRP3 in- ammasomes are re uired or athero enesis and activated by cholesterol crystals. *Nature.* 2010 464(7293) 1357-1361.
29. Masters SL Dunne A Subramanian SL et al. Activation o the NLRP3 in ammasome by islet amyloid polypeptide provides a mechanism or enhanced IL-1beta in type 2 diabetes. *Nat Immunol.* 2010 11(10) 897-904.
30. Vandanma sar B oum H Ravussin A et al. The NLRP3 in ammasome insti ates obesity-induced in ammation and insulin resistance. *Nat Med.* 2011 17(2) 179-188.
31. uliana C Fernandes-Alnemri T Wu et al. Anti- in ammatory compounds parthenolide and Bay 11-7082 are direct inhibitors o the in ammasome. *J Biol Chem.* 2010 285(13) 9792-9802.
32. Ai awa Hirabayashi Iwana a et al. - cient and accurate homolo ous recombination in h SCs and hiPSCs usin helper-dependent adenoviral vectors. *Mol Ther.* 2012 20(2) 424-431.
33. Soldner F La aniere Chen AW et al. eneration o iso enic pluripotent stem cells di erin e clusively at two early onset Par inson point mutations. *Cell.* 2011 146(2) 318-331.
34. Cheun A Horvath LM ra odats aya D et al. Isolation o M CP2-null Rett syndrome patient hiPS cells and iso enic controls throu h -chromosome inactivation. *Hum Mol Genet.* 2011 20(11) 2103-2115.
35. im Hysolli Par IH. Neuronal maturation de ect in induced pluripotent stem cells rom patients with Rett syndrome. *Proc Natl Acad Sci U S A.* 2011 108(34) 14169-14174.
36. Pomp Dreesen Leon DF et al. Une - pected chromosome s ewin durin culture and repro rammin o human somatic cells can be alleviated by e o enous telomerase. *Cell Stem Cell.* 2011 9(2) 156-165.
37. ore A Li Z Fun HL et al. Somatic codin mutations in human induced pluripotent stem cells. *Nature.* 2011 471(7336) 63-67.
38. Crotti L Lund uist AL Insolia R et al. CNH2- 897T is a enetic modi er o latent con enital lon - T syndrome. *Circulation.* 2005 112(9) 1251-1258.
39. Raya A Rodri ue -Pi a l uenechea et al. Disease-corrected haematopoietic pro enitors rom Fanconi anemia induced pluripotent stem cells. *Nature.* 2009 460(7251) 53-59.
40. Muller LU Milsom MD Harris C et al. ver- comin repro rammin resistance o Fanconi anemia cells. *Blood.* 2012 119(23) 5449-5457.

Critical Review

Toward an Understanding of Immune Cell Sociology: Real-Time Monitoring of Cytokine Secretion at the Single-Cell Level

Yoshitaka Shirasaki[1]
Mai Yamagishi[1]
Nanako Shimura[1]
Atsushi Hijikata[1]
Osamu Ohara[1,2]*

[1]Laboratory for Immunogenomics, RIKEN Research Center for Allergy and Immunology, Yokohama, Kanagawa, Japan
[2]Department of Human Genome Research, Kazusa DNA Research Institute, Kisarazu, Chiba, Japan

Abstract

The immune system is a very complex and dynamic cellular system, and its intricacies are considered akin to those of human society. Disturbance of homeostasis of the immune system results in various types of diseases; therefore, the homeostatic mechanism of the immune system has long been a subject of great interest in biology, and a lot of information has been accumulated at the cellular and the molecular levels. However, the sociological aspects of the immune system remain too abstract to address because of its high complexity, which mainly originates from a large number and variety of cell–cell interactions. As long-range interactions mediated by cytokines play a key role in the homeostasis of the immune system, cytokine secretion analyses, ranging from analyses of the micro level of individual cells to the macro level of a bulk of cell ensembles, provide us with a solid basis of a sociological viewpoint of the immune system. In this review, as the first step toward a comprehensive understanding of immune cell sociology, cytokine secretion of immune cells is surveyed with a special emphasis on the single-cell level, which has been overlooked but should serve as a basis of immune cell sociology. Now that it has become evident that large cell-to-cell variations in cytokine secretion exist at the single-cell level, we face a tricky yet interesting question: How is homeostasis maintained when the system is composed of intrinsically noisy agents? In this context, we discuss how the heterogeneity of cytokine secretion at the single-cell level affects our view of immune cell sociology. While the apparent inconsistency between homeostasis and cell-to-cell heterogeneity is difficult to address by a conventional reductive approach, comparison and integration of single-cell data with macroscopic data will offer us a new direction for the comprehensive understanding of immune cell sociology. © 2012 IUBMB Life, 65(1):28–34, 2013

Keywords: *immune system; cytokine; single cell; secretion; cell sociology*

Introduction

The immune system is one of the most dynamic and complex systems in biological systems. As is well known, the very basic function of the immune system is the discrimination between the self and non-self. Thus, the immune system is highly critical in guarding an organism from the invasion of various pathogenic agents as well as tumor cells. However, when immune cells behave abnormally, it could cause serious autoimmune diseases, because the immune system misrecognizes the self as a foreign enemy. To achieve such highly sophisticated functions, the immune system is composed of a large number and variety of cells dynamically regulated in space, time, and cell population. Because the number of immune cells in the human body is in the order of trillions, the complexity of the immune system may be as high as, or even higher than that of human society. Human sociology is an old multidisciplinary science, and its approaches are well developed. Thus, when attempting to tackle immune diseases, we must be prepared to examine the "sociology of the immune cells." There are various similarities between societies of human and immune cells from a sociological viewpoint; for example, modern human

Abbreviations: *IL, interleukin; LPS, lipopolysaccharide; IFN, interferon; CINCA, chronic infantile neurological cutaneous and articular syndrome*

Volume 65, Number 1, January 2013, Pages 28-34

**Address for correspondence to: Osamu Ohara, Laboratory for Immunogenomics, RIKEN Research Center for Allergy and Immunology, 1-7-22 Suehiro-cho, Tsurumi, Yomkohama, Kanagawa 230-0045, Japan. E-mail: oosamu@rcai.riken.jp.*

Received 28 August 2012; accepted 3 October 2012

DOI: 10.1002/iub.1110

Published online in Wiley Online Library (wileyonlinelibrary.com)

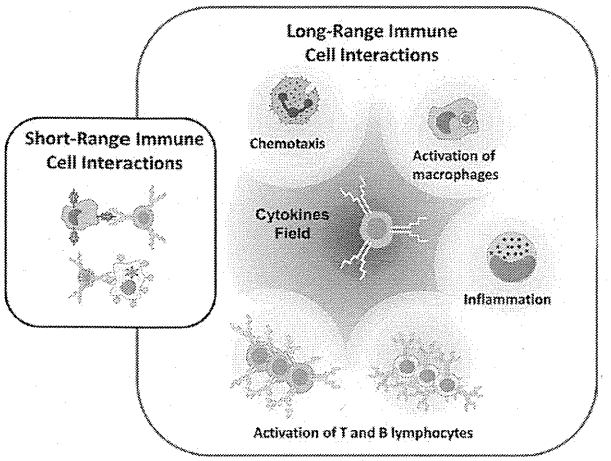

FIG 1 *In the immune system, short- and long-range interactions among cells play key roles in a variety of immune events. The short-range interactions are critical in a cell–cell recognition phase, which is followed by activation and effector phases. In the latter phases, the long-range interactions mediated by cytokines evoke a variety of cell functions such as macrophage activation, B- and T-cell activation, inflammation, and chemotaxis. Cell illustrations shown here were prepared with a PPT-Toolkit-Immunology from Motifolio (MD).*

communication systems remind us of cytokine signaling among immune cells. When considering immune cell sociology, we should carefully estimate (i) the variability of single cells in time and population and (ii) the social behavior of cells resulting from reciprocal interactions. Now that a wealth of information regarding cellular and molecular "parts" of immune systems has been amassed, it is time to start seriously considering how to approach the exciting concept of "immune cell sociology."

In general, the complexity of the system emerges from a variety of interactions among the constituents of the system. It is well known that cell–cell interactions play a pivotal role in the homeostasis of the immune system. Cell–cell interactions are classified into two groups, namely, short- and long-range interactions. A representative example of the short-range interactions is mediated by physical contact between cells via surface molecules (Fig. 1). In contrast, a majority of long-range interactions among cells are via humoral factors, whereas other mechanisms such as membrane nanotube and electric signals also work in some cases. In particular, cytokines serve as a representative set of humoral factors in the immune system, and they function as excellent mediators to convey cellular signals to cells, including those that are distantly positioned, because of their extremely low biologically effective concentration. The aim of this review is to outline current technologies for monitoring secretion processes of cytokines from immune cells, even at the single-cell level, and to raise a provocative discussion as to how the heterogeneity of immune cells in terms of cytokine secretion could affect the "social" behavior as a whole.

Cytokine Profiles of Immune Cells

Comprehensive analysis of secretory proteins, sometimes called "secretome" analysis, has been recently achieved by mass spectrometry (1). However, cytokine amounts are frequently below the practical detection limit of the most advanced proteome approaches based on mass spectrometry. Thus, antibody-based assays remain the gold standard for cytokine quantification. In addition, because an immunoassay system with multiplexity higher than 20 has become commercially available since the last decade, it is feasible to comprehensively monitor cytokine levels simultaneously. While these cytokine profiles of immune cells under various culture conditions must be informative when dealing with immune cell sociology, unfortunately, these data are dispersed in the literature. Thus, we performed cytokine profiling of immune cells by ourselves and made the information available on RefDIC (http://refdic.rcai.riken.jp), a website originally constructed to provide the research community with reference transcriptome/proteome datasets of immune cells. It enables researchers to browse cytokine profiles with mRNA profiles of cytokine and/or cytokine receptor genes in a comparative manner on the same platform (2). Figure 2 shows an example of clustering of cytokine profiles of mouse immune cells under different culture conditions (unpublished results). These data obtained by bulk assays should be very informative to enable the understanding of the state of a cell ensemble. However, it is unclear whether the cell ensemble is composed of a homogeneous population at this stage. To understand complex and dynamic behaviors of the immune system, behaviors of individual cellular agents are very critical from a sociological viewpoint. Although the analysis of protein secretion from single cells used to be highly challenging in the past, the situation has changed drastically, as described below.

Available Methods for Monitoring Protein Secretion from Single Cells

Single-cell analysis is a very active field in technology development (3), and many interesting methods have been developed. For example, single-cell mass cytometry dramatically increases the amounts of information obtained by a single experimental run than by conventional fluorescence-based cytometry, greatly contributing to the understanding of signal transduction systems (4). However, most of the methods are designed for intracellular biomolecules. Single-cell mRNA analysis has been used for estimating the expression of cytokines and/or other secretory proteins. However, as the

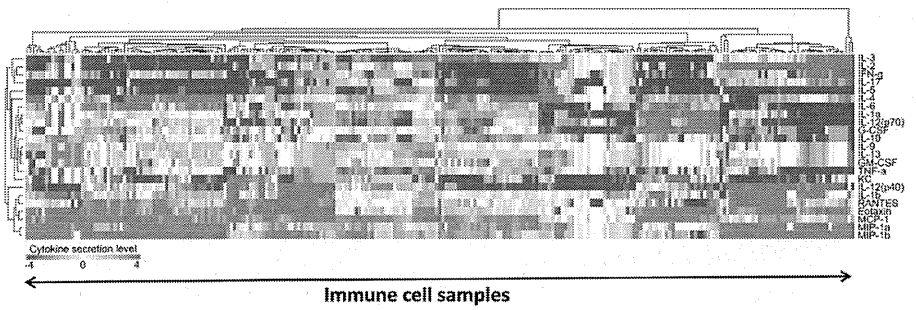

FIG 2 *Clustering of cytokine profiles of immune cells. As an example, cytokine profiles measured with a mouse Bio-Plex cytokine panel (Bio-Rad Laboratories, CA) are clustered and indicated as a heat map. Cytokine concentrations are median-normalized among samples and expressed as log_2 values of those divided by the median value. While cytokine profiles allow us to cluster each immune cell type separately, they are considerably modulated by external conditions as well.*

secretion of some cytokines—particularly proinflammatory cytokines such as those without conventional signal sequences—cannot be estimated from their mRNA levels, cytokine profiling should be done at the protein level. As for protein secretion, several single-cell methods have been also reported. Table 1 lists the methods reported in the relevant literature (5–10). Each method has its own advantages and disadvantages, as shown in Table 1. It is worth noting that all the methods shown here detect the secreted molecules as a snapshot. What kind of new information can be obtained by single-cell secretion assays? Figure 3 displays the typical data of single-cell secretion rates obtained by the microengraving method by our team (Shimura et al., manuscript in preparation). In this case, a macrophage-like cell line (J774.1 cells) was treated with lipopolysaccharide (LPS) and was monitored for the secretion rate of interleukin-6 (IL-6) between 4 and 5 h after the treatment. A conventional bulk assay of IL-6 demonstrated that J774.1 cells started to secrete IL-6 2 h after the treatment and kept increasing the secretion rate till 5 h. The data shown in Fig. 3 revealed that the secretion of IL-6 resulted from the increase in the number of secreting cells and the amounts of secreted IL-6 from each single cell. However, it should be noted that about 40% of the cells did not secrete IL-6 above the detection limit, even 4 h after the LPS stimulation, which cannot be seen from the bulk data. Thus, while many new, unaddressed questions arise from such data, it is evident that the immune cells respond to an external stimulation differently even in an ensemble of cloned, genetically identical cells. In our data, although the secretion profile and the time course of cytokine induction varied from cytokine to cytokine, none of the cytokine profiles became normally distributed.

Real-Time Monitoring of Cytokine Secretion from Single Immune Cells

As described above, the single-cell secretion assay revealed large cell variability in the population context, which is critical for a sociological viewpoint. However, the data are snapshots of the cell ensemble and do not provide us with information on

TABLE 1 ***Single-cell secretion assay systems***

Method	*Quantitativeness*	*Throughput/assay*	*Recovery of cells*	*Data type*[a]	*Reference*
Quantitative ELISpot	Low	$\sim 10^3$ cells	Impossible	Snapshot	(5)
Single-cell barcoding	High	$\sim 10^4$ cells	Impossible	Snapshot	(6)
Immunospot array chip	Low	$>10^5$ cells	Possible	Snapshot	(7)
Microengraving	High	$>10^5$ cells	Possible	Snapshot	(8)
Gel microdrop assay	Medium	$>10^6$ cells	Possible	Snapshot	(9)
Cytometric cytokine secretion assay	Medium	$>10^6$ cells	Possible	Snapshot	(10)

[a] *Secreted proteins are not detected simultaneously with the secretion process but are detected postreaction with the labeled detection antibody.*

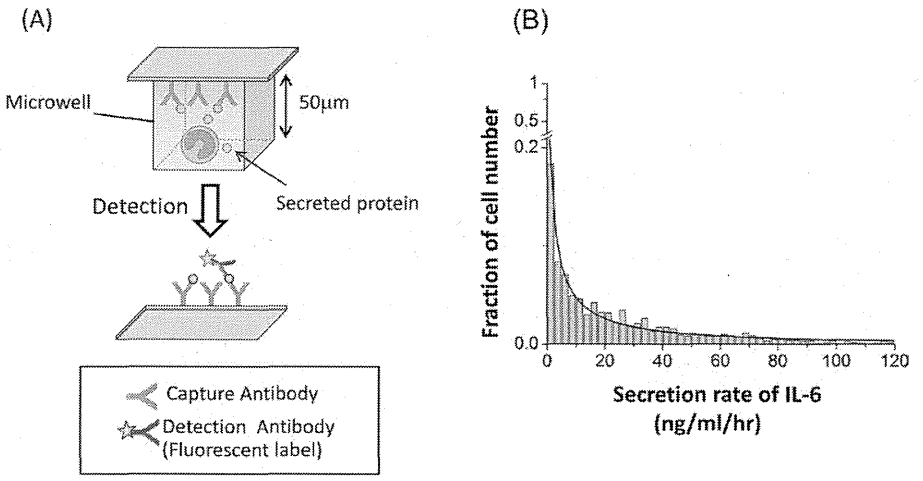

FIG 3 *Population distribution of IL-6 secretion rates after LPS induction. (A) The principle of the microengraving method (8) is illustrated. In a closed microwell, cells are allowed to secrete proteins, which are captured by capture antibodies on a solid support. After incubation for a specified time, the bound secreted proteins are quantified by fluorescence intensities from detection antibodies on the solid support. (B) The population distribution of IL-6 secretion rates of J774.1 cells was obtained by the microengraving method. The secretion rates shown here are calculated from the accumulated amounts of IL-6 secreted between 4 and 5 h after LPS stimulation.*

cell dynamics. The single-cell dynamics along time is another important property (11), and it also has great significance in the field of immune cell sociology. While large cell-to-cell variations in cytokine secretion rate were observed on a snapshot in the population context as described above, we cannot know how stable such a biased distribution of cytokine secretion rates is. Just in case the cell heterogeneity of cytokine secretion rates can be averaged within a time range of cellular events, it may not be so critical from a sociological viewpoint. In this regard, we have already developed a real-time monitoring system for antigen–antibody complexes in picoliter-scale microwells (12) and have modified it for monitoring protein secretion. In addition, we considered the following two points in developing the real-time monitoring system: (i) intracellular events can also be monitored, when necessary, in parallel with the detection of secreted molecules and (ii) cells can be retrieved at a specified timing. For these purposes, a new microwell device equipped with total internal reflection illumination was produced (13). While methodological details of this method will be reported later (Shirasaki et al., manuscript in preparation), this new system, for the first time, enables simultaneous monitoring of cytokine secretion and intracellular events (anything seen on the same microscopy platform, such as translocation of transcription factors, membrane intactness, changes in Ca^{2+} concentration, etc.) in real time, as well as the analysis of mRNA/protein levels of a single cell at the time of interest. In particular, it should be emphasized that the monitoring of protein secretion is absolutely compatible with bioimaging.

By using the real-time monitoring system, we can follow the changes in cytokine secretion along time. Figure 4 shows a snapshot of the assay where the secretion of two cytokines (IL-6 and CCL2) from MC/9 cells, a mast cell-like cell line, were simultaneously monitored, indicating that secretion rates of the two cytokines have a low correlation with each other. Because these two cytokines are induced by treatment with a phorbol ester, MC/9 cells respond differently to the external signal in terms of IL-6 and CCL2 secretion. Because the low correlation of secretion rates of multiple cytokines thought to be under the same induction pathway is frequently observed, it is very likely that cell heterogeneity in cytokine secretion originates from stochasticity. Although it is not evident from Fig. 4, our data indicated that the stochastic differences in cytokine secretion at the single-cell level lasted for more than 8 h. As demonstrated in this example, it now becomes possible to delineate cytokine secretion from single cells not only in a population context but also with time.

How Does Heterogeneity of Cytokine Secretion of Immune Cells Affect Our View of Immune Cell Sociology?

In general, cell heterogeneity could originate from (i) stochasticity, (ii) epigenetic factors, or (iii) genetic factors, while heterogeneity in external conditions and cell cycle state may also affect it to some extent. In experiments using a cloned cell population, cell-to-cell variations are most likely to be derived mainly from the stochasticity of multilayered processes, including transcription, translation, and protein transfer. After a pioneering study by Ko (14), stochasticity in gene expression is

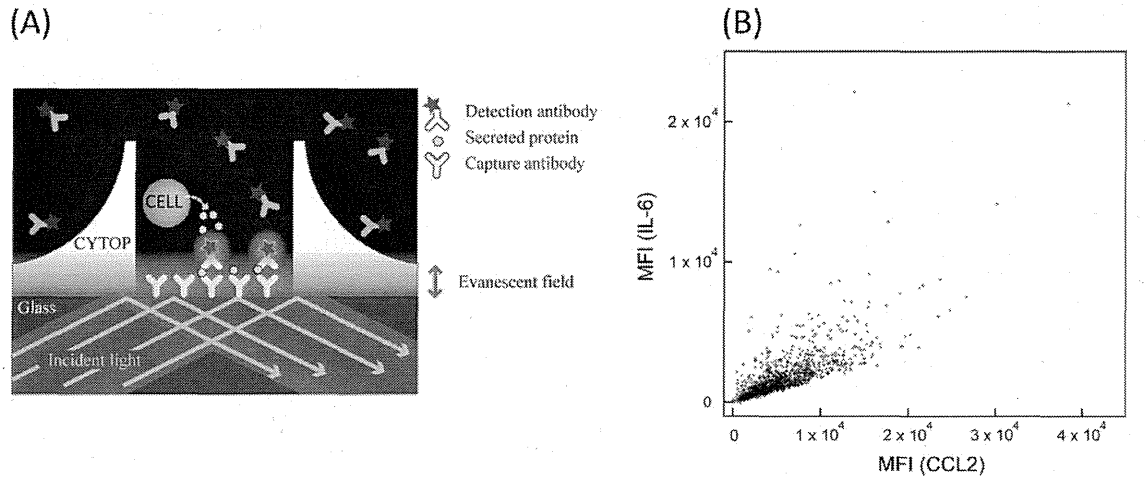

FIG 4

Simultaneous measurements of secretion of IL-6 and CCL2 in real-time. Principle of real-time monitoring system of protein secretion from a single cell. A microwell is fabricated with Cytop to enable us to detect protein secretion in real-time by total internal reflection illumination, as described (12). Fluorescent sandwich complexes of secreted protein and antibodies captured on the solid support are quantified. The top of the microwell is open for the following two reasons: to keep cells healthy during observation and to allow cell retrieval at the time specified. Detection of IL-6 and CCL2 secretion from MC/9 cells after treatment with a phorbol ester. The secretion of IL-6 and CCL2 from single MC/9 cells 4 h after treatment with a phorbol ester is illustrated. Each dot indicates medians of fluorescence intensity (MFI) of IL-6 and CCL2 signals form a single cell. As shown, the ratio of MFIs varied widely from cell to cell.

being actively explored (15). It is widely accepted that transcription/translation processes are stochastic at the single-cell level, which is no surprise because these processes are governed by a relatively small number of molecules. In other words, cell responses are intrinsically noisy. Thus, an important and obvious question is how the immune system maintains homeostasis when using such noisy cells.

What kind of new insights can we get from these new lines of information? From a viewpoint of immune cell sociology, the cause of cell heterogeneity does not matter but its dynamics does. We have vaguely assumed that such a stochastic effect does not last long; however, our data, as well as those reported by other groups, indicate that it takes relatively long (hours to days) (16,17). Thus, when we consider immune events responding within a short range of time (i.e., hours), the cell-to-cell variations caused even by stochastic transcription/translation cannot be neglected at all. An analytical framework for linking stochastic dynamics to population distribution was discussed by Friedman et al. (18), and the real situation was described as being more complex, thus necessitating experimental measurements to understand it at the single-cell level.

Rand et al. (19) reported that the key steps of virus-induced signal transduction, interferon (IFN)-beta expression, and the induction of IFN-stimulated genes take place stochastically. According to the authors, the origin of stochasticity seems to be cell-intrinsic noise in transcription and/or translation. Coherent, robust, antiviral protection in spite of multilayered cellular stochasticity is explained to be achieved through intercellular communication, which is likely to be a widely used strategy by mammalian cells to cope with pervasive stochastic signaling and gene expression. However, in this scenario, cell-intrinsic noise is considered disadvantageous for the cell society. Is this always the case? In fact, as long as we consider events that protect cells from destruction, heterogeneity might be undesirable, because the number of cells protected becomes smaller than the coherent cell ensemble. However, if all the cells are subjected to extracellular attacks to induce cell death, heterogeneity might have a positive meaning, because at least a small fraction of cells might survive and save the whole system. Because cytokines play a key role in communication among immune cells, cell-to-cell variations in cytokine secretion could be a strategy to make the "society" flexible and tough in some cases.

The other two reasons, epigenetic and genetic causes, which may generate cell-to-cell variations, are equally or more important than stochasticity from a viewpoint of immune cell sociology. Epigenetic variations are actively explored in their action and regulation at present and will offer us intriguing pieces of information on immune cell sociology. Epigenetic differences frequently result in differences in cell types, which offer a conceptual basis for each immune cell type in conventional immune cell sociology. When epigenetically different cells are functionally distinct, they are conventionally designated as different cell modules (i.e., helper T cells, B cells, NK cells, etc.) in immune cell society. While it has been a relatively macroscopic view, such heterogeneities have been accounted for in immunology.

Genetic variations may be practically more important than stochasticity and genetic factors. A well-known example is found in cancer, where a somatic mutation is first introduced in a very limited number of cells, and the mutant cells are killed, maintained, or expanded under the surveillance by the immune system (20). This is really a matter of immune cell sociology. Another interesting example is found in autoinflammatory disease, a type of primary immunodeficiency disease. Chronic infantile neurological cutaneous and articular syndrome (CINCA), also known as neonatal-onset multisystem inflammatory disease, is characterized by urticarial rash, neurological manifestations, and arthropathy. This dominantly inherited systemic autoinflammatory disease is provoked by somatic mosaicism of gain-of-function NLRP3 mutations as well as a heterozygous germline mutation (21). Furthermore, we recently reported a reliable genetic diagnostic method using massive, parallel DNA sequencing (22). The mutation of NLRP3 activates the inflammasome and is considered to result in the release of a large amount of IL-1β. Thus, in the presence of even a small fraction of mutated cells, CINCA patients might develop a fever. This may be a good example that a small fraction of anomalously behaving cells leads the whole body to a diseased state. Thus, somatic mutation-induced diseases like the CINCA syndrome may serve as a good model to explore how the homeostasis is interrupted or maintained in the presence of such cellular heterogeneity. In this regard, it is interesting to note that periodic fever is observed in CINCA patients, because the oscillating biological events have been actively studies by mathematical modeling for long time (23).

Now that it has become feasible to monitor secretory proteins, as well as intracellular ones at the single-cell level, we can delve into the details of immune cell society at the microscopic level, that is, at the single-cell resolution, if we want. Although such a microscopic analysis might not be always necessary, it must be highly informative, particularly in those cases where the whole system is affected by a small group of heterogeneous immune cells. In such cases, the long-range cellular interactions mediated by cytokines must play a key role. We anticipate that it might unravel a new paradigm of immune cell sociology.

Future Perspectives of the Cell–Cell Interactome at the Single-Cell Level: What are the Implications for Immune Cell Sociology?

The term "cell sociology" was first used in the field of morphogenesis (24). In this review, the term is used for the demonstration of orderliness rather than the dynamic nature of the biological system. Although the term "cell sociology" may be considered an equivalent of "systems biology" in some contexts in this review, we intentionally use it to emphasize the complexity and dynamics of the system. For instance, modern human society has become highly global and dynamic as a consequence of people connecting and interacting via the internet, which is analogous to the situation of the immune system governed by long-range interactions with cytokines. Similarly, the study of how proteins interact with each other and are spatially arranged is designated as "molecular sociology" (25), which also has the sole emphasis on the importance of the complex interactions among common constituents of the "society." In this regard, short-range interactions mediated by cell–cell contact may be analogous to face-to-face communications in human, which are observed even in primitive society. The issue of how homeostasis is maintained with intrinsically noisy agents is an interesting aspect to address, and it might be analogous to the stabilization of the human society, which comprises considerably heterogeneous individuals from a sociological viewpoint. In both cases, as far as long-range interactions are functioning, individuality can be harnessed such that the system as a whole responds to external perturbations in a harmonious and robust manner.

In this context, to get a comprehensive understanding of the immune system, we propose to take sociological approaches in immunological studies. A good lesson to learn from sociology is that it is a multidisciplinary and multiscale science; many different approaches, ranging from micro level to macro level, are eventually integrated to interpret a variety of social events. In the case of immune cell sociology, regulation of long-range interactions among immune cells must be a critical issue, requiring an understanding at the micro level of individual cell agents, as well as the macro level, where the immune events are explained as a consequence of interactions among immune cellular modules (i.e., functional cellular ensembles with particular cellular designations). While immune cell sociology at the macro level has a long and successful history and is already well developed, advances of single-cell analysis technologies enable us to decipher the interactome of immune cells at a deeper resolution. What is expected is to integrate these multiscale data into a sociological view of the immune system. Although still in infancy, interactome analysis of immune cells at the single-cell level might elucidate unexpected mechanisms underlying the maintenance and destruction of immune homeostasis in the future, which would enable us to develop a new way to tackle various immune diseases.

References

[1] Stastna, M. and Van Eyk, J. E. (2012) Secreted proteins as a fundamental source for biomarker discovery. Proteomics 12, 722–735.

[2] Hijikata, A., Kitamura, H., Kimura, Y., Yokoyama, R., Aiba, Y., et al. (2007) Construction of an open-access database that integrates cross-reference information from the transcriptome and proteome of immune cells. Bioinformatics 23, 2934–2941.

[3] de Souza, N. (2011) Single-cell methods. Nat. Methods 9, 35–35.

[4] Bendall, S. C., Simonds, E. F., Qiu, P., Amir el, A. D., Krutzik, P. O., et al. (2011) Single-cell mass cytometry of differential immune and drug responses across a human hematopoietic continuum. Science 332, 687–696.

[5] Henn, A. D., Rebhahn, J., Brown, M. A., Murphy, A. J., Coca, M. N., et al. (2009) Modulation of single-cell IgG secretion frequency and rates in human memory B cells by CpG DNA, CD40L, IL-21, and cell division. J. Immunol. 183, 3177–3187.
[6] Ma, C., Rong, F., AhmadH., Shi, Q., Comin-Anduix, B., et al. (2011) A clinical microchip for evaluation of single immune cells reveals high functional heterogeneity in phenotypically similar T cells. Nat. Med. 17, 738–743.
[7] Jin, A., Ozawa, T., Tajiri, K., Obata, T., Kondo, S., et al. (2009) A rapid and efficient single-cell manipulation method for screening antigen-specific antibody-secreting cells from human peripheral blood. Nat. Med. 15, 1088–1092.
[8] Love, J. C., Ronan, J. L., Grotenbreg, G. M., van der Veen, A. G., and Pleogh, H. L. (2006) A microengraving method for rapid selection of single cells producing antigen-specific antibodies. Nat. Biotechnol. 24, 703–707.
[9] Powell, K. T. and Weaver, J. C. (1990) Gel microdroplets and flow cytometry: rapid determination of antibody secretion by individual cells within a cell population. Biotechnology 8, 333–337.
[10] Manz, R., Assenmacher, M., Pfluger, E., Miltenyi, S., and Radbruch, A. (1995) Analysis and sorting of live cells according to secreted molecules, relocated to a cell-surface affinity matrix. Proc. Natl. Acad. Sci. USA 92, 1921–1925.
[11] Spiller, D. G., Wood, C. D., Rand, D. A., and White, M. R. (2010) Measurement of single-cell dynamics. Nature 465, 736–745.
[12] Sasuga, Y., Iwasawa, T., Terada, K., Oe, Y., Sorimachi, H., et al., (2008) Single-cell chemical lysis method for analyses of intracellular molecules using an array of picoliter-scale microwells. Anal. Chem. 80, 9141–9149.
[13] Nakahara, A., Shirasaki, Y., Kawai, K., Ohara, O., Mizuno, J., et al. (2011) Fabrication of high-aspect-ratio amorphous perfluorinated polymer structure for total internal reflection fluorescence microscopy. Microelectron. Eng. 8, 1817–1820.
[14] Ko, M. S. (1992) Induction mechanism of a single gene molecule: stochastic or deterministic? Bioessays 14, 341–346.
[15] Li, G. W. and Xie, X. S. (2011) Central dogma at the single-molecule level in living cells. Nature 475, 308–315.
[16] Suter, D. M., Molina, N., Gatfield, D., Schneider, K., Schibler, U., et al. (2011) Mammalian genes are transcribed with widely different bursting kinetics. Science 332, 472–474.
[17] Chang, H. H., Hemberg, M., Barahona, M., Ingber, D. E., and Huang, S. (2008) Transcriptome-wide noise controls lineage choice in mammalian progenitor cells. Nature 453, 544–547.
[18] Friedman, N., Cai, L., and Xie, X., (2006) Linking stochastic dynamics to population distribution: an analytical framework of gene expression. Phys. Rev. Lett. 97, 168302.
[19] Rand, U., Rinas, M., Schwerk, J., Nohren, G., Linnes, M., et al. (2012) Multi-layered stochasticity and paracrine signal propagation shape the type-I interferon response. Mol. Syst. Biol. 8, 584.
[20] Xu, X., Hou, Y., Yin, X., Bao, L., Tang, A., et al. (2012) Single-cell exome sequencing reveals single-nucleotide mutation characteristics of a kidney tumor. Cell 148, 886–895.
[21] Tanaka, N., Izawa, K., Saito, M. K., Sakuma, M., Oshima, K., et al. (2011) High incidence of NLRP3 somatic mosaicism in patients with chronic infantile neurologic, cutaneous, articular syndrome: results of an International Multicenter Collaborative Study. Arthritis Rheum. 63, 3625–3632.
[22] Izawa, K., Hijikata, A., Tanaka, N., Kawai, T., Saito, M. K., et al. (2012) Detection of base substitution-type somatic mosaicism of the NLRP3 gene with >99.9% statistical confidence by massively parallel sequencing. DNA Res. 19, 143–152.
[23] Mackey, M. C. and Glass, L. (1977) Oscillation and chaos in physiological control system. Sci. China Life Sci. 197, 287–289.
[24] Chandebois, R. (1976) Cell sociology: a way of reconsidering the current concepts of morphogenesis. Acta Biotheor. 25, 71–102.
[25] Robinson, C. V., Sali, A., and Baumeister, W. (2007) The molecular sociology of the cell. Nature 450, 973–982.

Wnt3a stimulates maturation of impaired neutrophils developed from severe congenital neutropenia patient-derived pluripotent stem cells

Takafumi Hiramoto[a,b], Yasuhiro Ebihara[b,c,1], Yoko Mizoguchi[d], Kazuhiro Nakamura[d], Kiyoshi Yamaguchi[e], Kazuko Ueno[f], Naoki Nariai[f], Shinji Mochizuki[b,c], Shohei Yamamoto[b,c], Masao Nagasaki[f], Yoichi Furukawa[e], Kenzaburo Tani[a], Hiromitsu Nakauchi[g], Masao Kobayashi[d], and Kohichiro Tsuji[b,c]

[a]Division of Molecular and Clinical Genomics, Medical Institute of Bioregulation, Kyushu University, Higashi-ku, Fukuoka 812-8582, Japan; [c]Department of Pediatric Hematology/Oncology, Research Hospital, Divisions of [b]Stem Cell Processing and [g]Stem Cell Therapy, Center for Stem Cell Biology and Regenerative Medicine, and [e]Division of Clinical Genome Research, Advanced Clinical Research Center, Institute of Medical Science, University of Tokyo, Minato-ku, Tokyo 108-8639, Japan; [d]Pediatrics, Hiroshima University Graduate School of Biomedical and Health Sciences, Minami-ku, Hiroshima 734-8551, Japan; and [f]Department of Integrative Genomics, Tohoku Medical Megabank Organization, Tohoku University, Aramaki, Aoba-ku, Sendai 980-8573, Japan

Edited by George Q. Daley, Children's Hospital Boston, Boston, MA, and accepted by the Editorial Board January 4, 2013 (received for review October 1, 2012)

The derivation of induced pluripotent stem (iPS) cells from individuals of genetic disorders offers new opportunities for basic research into these diseases and the development of therapeutic compounds. Severe congenital neutropenia (SCN) is a serious disorder characterized by severe neutropenia at birth. SCN is associated with heterozygous mutations in the neutrophil elastase [elastase, neutrophil-expressed (ELANE)] gene, but the mechanisms that disrupt neutrophil development have not yet been clarified because of the current lack of an appropriate disease model. Here, we generated iPS cells from an individual with SCN (SCN-iPS cells). Granulopoiesis from SCN-iPS cells revealed neutrophil maturation arrest and little sensitivity to granulocyte-colony stimulating factor, reflecting a disease status of SCN. Molecular analysis of the granulopoiesis from the SCN-iPS cells vs. control iPS cells showed reduced expression of genes related to the wingless-type mmtv integration site family, member 3a (Wnt3a)/β-catenin pathway [e.g., lymphoid enhancer-binding factor 1], whereas Wnt3a administration induced elevation lymphoid enhancer-binding factor 1-expression and the maturation of SCN-iPS cell-derived neutrophils. These results indicate that SCN-iPS cells provide a useful disease model for SCN, and the activation of the Wnt3a/β-catenin pathway may offer a novel therapy for SCN with ELANE mutation.

apoptosis | unfolded protein response | SCN disease model

Severe congenital neutropenia (SCN) is a heterogeneous bone marrow (BM) failure syndrome characterized by severe neutropenia at birth, leading to recurrent infections by bacteria or fungi (1). SCN patients reveal an arrest in neutrophil differentiation in the BM at the promyelocyte or myelocyte stage (1), as well as a propensity to develop myelodysplastic syndrome and acute myeloid leukemia (2). Current treatment by high-dose granulocyte-colony stimulating factor (G-CSF) administration induces an increase in the number of mature neutrophils in the peripheral blood of most SCN patients (3). Although this treatment is curative for the severe infections, there is a concern that high-dose G-CSF may increase the risk of hematologic malignancy in these individuals (4).

Several genetic mutations have been identified in SCN patients. Approximately 50% of autosomal-dominant SCN cases were shown to have various heterozygous mutations in the gene encoding neutrophil elastase [elastase, neutrophil-expressed (ELANE)] (5, 6), a monomeric, 218-amino acid (25 kDa) chymotryptic serine protease (7) that is synthesized during the early stages of primary granule production in promyelocytes (8, 9). However, the mechanism(s) causing impaired neutrophil maturation in SCN patients remains unclear due to the current lack of an appropriate disease model.

Results and Discussion

In the present study, we generated induced pluripotent stem (iPS) cells from the BM cells obtained from an SCN patient with a heterologous ELANE gene mutation (exon 5, 707 region, C194X) (SCN-iPS cells) to provide the basis for an SCN disease model. The patient who donated BM cells recurrently suffered from severe infections without exogenous G-CSF administration, but the G-CSF administration once a week prevented his repeated infection. The SCN-iPS cells continued to show embryonic stem cell morphology after >20 passages and also expressed pluripotent markers (Fig. S1*A*). The silencing of exogenous genes and the capability to differentiate into three germ layers by teratoma formation were confirmed for each of the three SCN-iPS cell clones (Fig. S1 *B* and *C*). Furthermore, the same ELANE gene mutation that was present in the patient persisted in the SCN-iPS cells (Fig. S1*D*). The SCN-iPS cells, as well as control iPS cells that were generated from healthy donors, had the normal karyotype (Fig. S1*E*) (10, 11) and no mutations in the mutation-sensitive region of the G-CSF receptor gene (12).

We first compared the hematopoietic differentiation from SCN-iPS cells with that from control iPS cells that were generated from healthy donors. SCN-iPS and control iPS cells were cocultured with a 15-Gy-irradiated murine stromal cell line (the AGM-S3 cell line), as reported (13). After 12 d, the cocultured cells were harvested, and the $CD34^+$ cells separated from these cells (SCN-iPS–$CD34^+$ and control iPS–$CD34^+$ cells, respectively) were cultured in a hematopoietic colony assay by using a cytokine mixture (*Materials and Methods*). The number and size of the erythroid (E) and mixed-lineage (Mix) colonies derived from SCN-iPS–$CD34^+$ cells (1×10^4 cells) were nearly identical to those of the corresponding colonies derived from control iPS–$CD34^+$ cells (E colonies: SCN-iPS cells, 11.0 ± 3.0, and control iPS cells, 11.4 ± 3.9; Mix colonies: SCN-iPS cells, 25.1 ± 7.2, and control iPS cells, 17.4 ± 4.0) (Fig. 1 *B* and *C* and Fig. S2 *A* and *B*). However, the number of myeloid colonies derived from SCN-iPS–$CD34^+$ vs. control iPS–$CD34^+$ cells was significantly lower (SCN-iPS cells, 47.4 ± 19.5; control iPS cells, 127.8 ± 17.9; $P < 0.01$), and the size of the colonies was also smaller (Fig. 1 *A*

Author contributions: T.H., Y.E., K.Y., S.M., S.Y., Y.F., K. Tani, H.N., M.K., and K. Tsuji designed research; T.H., Y.M., K.N., and K.Y. performed research; T.H., Y.E., Y.M., K.N., K.Y., K.U., N.N., S.M., S.Y., M.N., and K. Tsuji analyzed data; and T.H., Y.E., and K. Tsuji wrote the paper.

The authors declare no conflict of interest.

This article is a PNAS Direct Submission. G.Q.D. is a guest editor invited by the Editorial Board.

[1]To whom correspondence should be addressed. E-mail: ebihara@ims.u-tokyo.ac.jp.

This article contains supporting information online at www.pnas.org/lookup/suppl/doi:10.1073/pnas.1217039110/-/DCSupplemental.

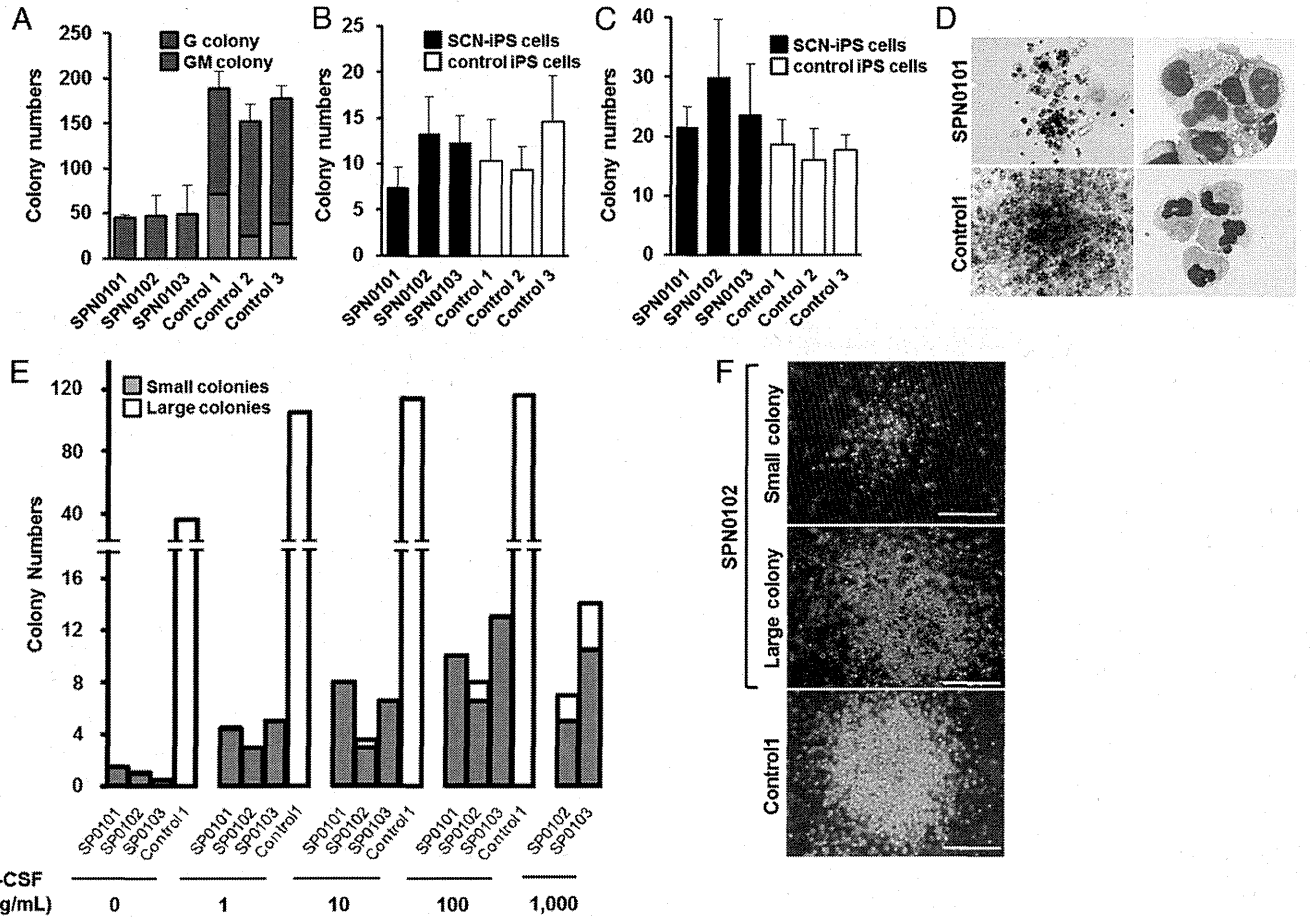

Fig. 1. Impaired neutrophil development from SCN-iPS cells. (*A–C*) A hematopoietic colony assay was performed by using 1×10^4 $CD34^+$ cells derived from three SCN-iPS cell clones (SPN0101, SPN0102, and SPN0103) and three control iPS cell clones (controls 1, 2, and 3) in the presence of a cytokine mixture. Colonies were sorted as myeloid (*A*), erythroid (*B*), and mixed-lineage (Mix) (*C*). Data are shown as mean ± SD. (*D*) Photographs of colonies (*Left*; 100×) and cells in a GM colony (*Right*; 400×; May–Grünwald–Giemsa staining). (*E*) A hematopoietic colony assay with dose escalation of G-CSF was performed by using 1×10^5 $CD34^+$ cells derived from SCN-iPS and control iPS cells. Filled and open bars indicate small colonies consisting of <100 cells and large colonies consisting of >100 cells, respectively. Data are shown as the average of three independent experiments. (*F*) Photographs of a small colony derived from SCN-iPS cells (SPN0102) in the presence of 10 ng/mL G-CSF, large colonies derived from SCN-iPS cells in the presence of 1,000 ng/mL G-CSF, and large colonies derived from control iPS cells (control 1) in the presence of 10 ng/mL G-CSF. (Scale bars, 200 μm.)

and *D*). In particular, only a few SCN-iPS cell-derived granulocyte (G) colonies—myeloid colonies consisting of only granulocytes—were detected (Fig. 1*A*). SCN-iPS cell-derived granulocyte–macrophage (GM) colonies—myeloid colonies consisting of macrophages/monocytes with/without granulocytes—contained a few immature myeloid cells in addition to macrophages/monocytes, whereas control iPS cell-derived GM colonies included a substantial number of mature, segmented, and band neutrophils (Fig. 1*D*).

We also found that Mix colonies derived from SCN-iPS cells, but not control iPS cells, contained immature myeloid cells and few mature neutrophils (Fig. S2 *C* and *D*). Next, we conducted a hematopoietic colony assay using various concentrations of G-CSF alone instead of the cytokine mixture to examine the G-CSF dose dependency of neutrophil differentiation from SCN-iPS and control iPS–$CD34^+$ cells. For all concentrations of G-CSF used (1–1,000 ng/mL), the SCN-iPS cell-derived myeloid colonies were significantly lower in number and smaller in size than the control iPS cell-derived myeloid colonies (Fig. 1*E*). Myeloid colony formation from control iPS cells reached a plateau at ~1–10 ng/mL G-CSF, whereas the number and size of those from SCN-iPS cells gradually increased with increasing concentrations of G-CSF. However, the values observed for SCN-iPS cells did not reach those for the control iPS cells, even at the highest dose of G-CSF used (1,000 ng/mL). Furthermore, large colonies consisting of >100 cells derived from SCN-iPS cells were only found with higher concentrations of G-CSF (Fig. 1*F*). Thus, granulopoiesis initiated from SCN-iPS cells was relatively insensitive to G-CSF, reflecting the inadequate in vivo response of neutrophils to G-CSF in SCN patients (14, 15). Therefore, these results support the applicability of the SCN-iPS cells established herein as a disease model for SCN.

To examine neutrophil development from SCN-iPS cells in more detail, SCN-iPS and control iPS–$CD34^+$ cells (1×10^4 cells each) were cocultured in suspension with AGM-S3 cells in the presence of neutrophil differentiation medium (*SI Materials and Methods*). The number of nonadherent cells derived from SCN-iPS–$CD34^+$ cells was lower than that from control iPS–$CD34^+$ cells on day 14 of culture (SCN-iPS cells, $9.77 \times 10^4 \pm 1.65 \times 10^4$ cells; control iPS cells, $52.48 \times 10^4 \pm 23.13 \times 10^4$ cells; $P < 0.05$) (Fig. 2*A*). The proportion of mature neutrophils among the nonadherent cells was also significantly lower for SCN-iPS cells relative to control iPS cells on day 14 (SPN-iPS cells, 15.53% ± 4.33%; control iPS cells, 71.285 ± 3.30%; $P < 0.05$) (Fig. 2 *B* and *C*), indicating that myeloid cells derived from SCN-iPS cells revealed the maturation arrest in the neutrophil development. We then examined a possibility that the maturation arrest in SCN-

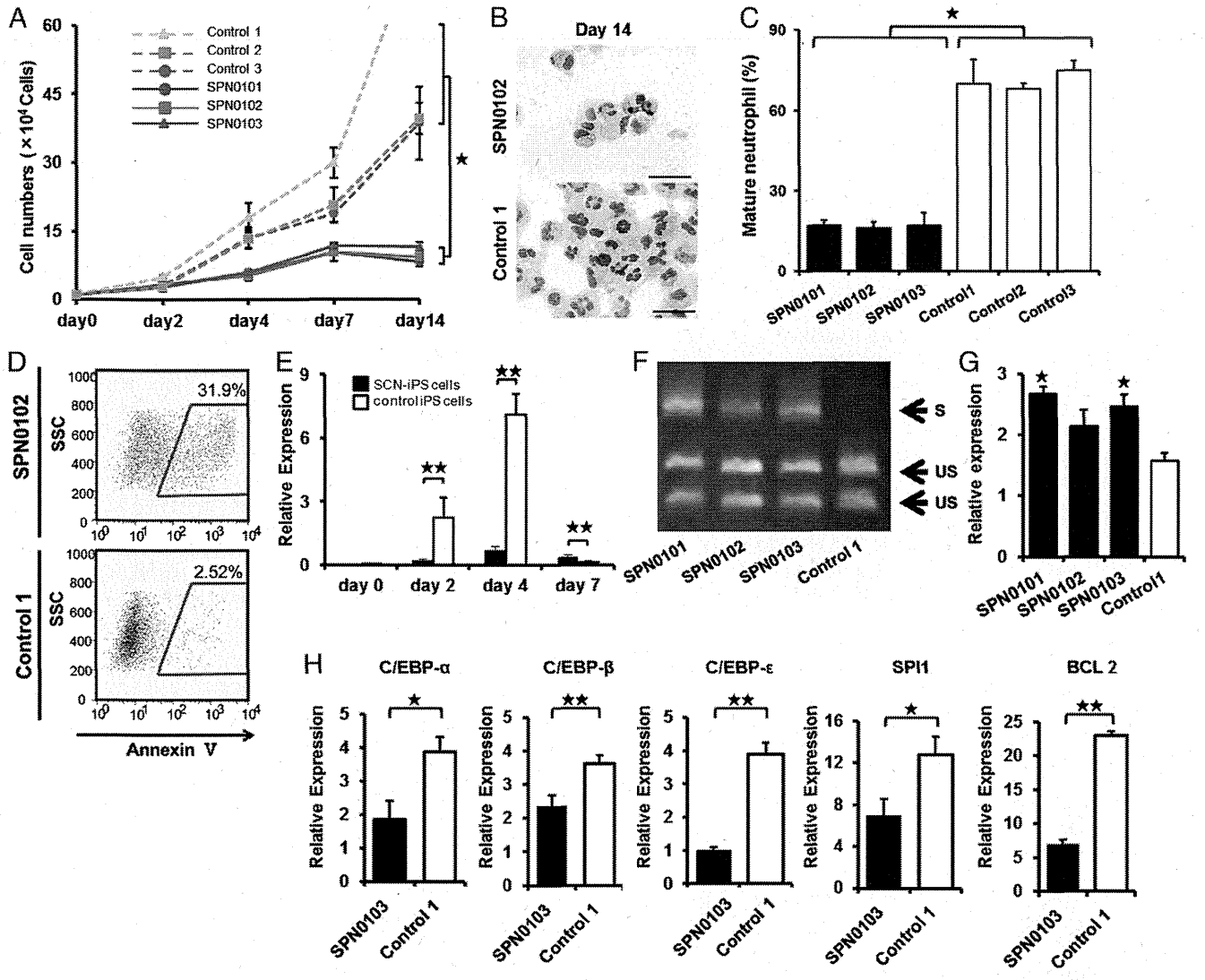

Fig. 2. Analysis of impaired neutrophil development from SCN-iPS cells. (*A*) Total number of nonadherent cells in the suspension culture of 1×10^4 $CD34^+$ cells derived from SCN-iPS and control iPS cells. Data are shown as mean ± SD. $^*P < 0.01$. (*B*) Photographs of nonadherent cells derived from SCN-iPS (SPN0103) and control iPS cells (control 1) on day 14 of culture (400×; May–Grünwald–Giemsa staining; scale bars, 50 μm.) (*C*) Filled and open bars show the proportion of mature neutrophils among the cells derived from SCN-iPS (filled bars) and control iPS (open bars) cells on day 14 of suspension culture. Data are shown as mean ± SD. $^*P < 0.05$. (*D*) Flow cytometric analysis of annexin V expression on cultured cells from SCN-iPS cells (SPN0102) or control iPS cells (control 1) on day 7. (*E*) Sequential qRT-PCR analysis of the relative expression of ELANE mRNA [ELANE/hypoxanthine–guanine phosphoribosyltransferase (HPRT) expression]. Data obtained from independent experiments using three SCN-iPS cell clones (SPN0101, SPN0102, and SPN0103) and three control iPS cell clones are shown as mean ± SD. $^{**}P < 0.01$. (*F* and *G*) $CD34^+$ cells derived from SCN-iPS or control iPS cells were cultured in neutrophil differentiation medium (see text). On day 7, nonadherent cells were collected and analyzed. (*F*) Representative gel showing spliced (S) and unspliced (US) XBP-1 bands on day 7. (*G*) qRT-PCR analysis of the relative mRNA expression (target/HPRT expression) of BiP on day 7. Data are shown as mean ± SD. $^*P < 0.05$; different from control 1). (*H*) qRT-PCR analysis of the relative mRNA expression (target / HPRT expression) of C/EBP-α, C/EBP-β, C/EBP-ε, SPI1, and BCL2 genes in non-adherent cells derived from SCN-iPS cells (filled bars, SPN0103) and control iPS cells (open bars, control 1) on day 2 of suspension culture. Data are shown as the mean ± the s.d. ($^{**}P < 0.01$, $^*P < 0.05$).

iPS cell-derived myeloid cells might be caused by their apoptosis. In flow cytometric analysis, SCN-iPS cell-derived myeloid cells contained a significantly higher proportion of annexin V-positive cells than control iPS-derived myeloid cells on day 7 of culture, suggesting that the maturation arrest in myeloid cells derived from SCN-iPS cells might be caused by their apoptosis (Fig. 2*D*).

We next examined ELANE mRNA expression levels in nonadherent cells derived from SCN-iPS vs. control iPS cells (Fig. 2*E*). ELANE expression was significantly lower in nonadherent cells derived from SCN-iPS vs. control iPS cells on days 2 and 4 of culture ($P < 0.01$), as reported (16, 17). However, the former was a little higher than the latter on day 7 ($P < 0.01$). This result may be explained by the existence of SCN-iPS cell-derived myeloid cells arrested at an early stage along the neutrophil differentiation pathway even on day 7 of culture. We also examined the expression of proteinase 3 and azurocidin, which comprise a family of closely related genes encoding neutrophil granule proteins along with ELANE, and found these genes were more highly expressed on day 4 (Fig. S3).

It has been reported that induction of the endoplasmic reticulum stress (ER) response and the unfolded protein response (UPR) has been advanced as a potential explanation for the molecular pathogenesis of SCN (18, 19). Thus, we examined activation of the UPR by X-box binding protein 1 (XBP-1) mRNA splicing on day 7. As shown in Fig. 2*F*, SPN-iPS cells induced XBP-1 mRNA splicing. We also found the up-regulation of BiP

(also known as GRP78 or HSPA5) (Fig. 2*G*). These results suggested that ER stress response and UPR might be involved in the pathogenesis in SCN.

To examine further the differences in gene expression between the two cell types, a microarray analysis was carried out by using $CD34^+$ cells derived from SCN-iPS and control iPS cells (three clones of each) in suspension culture on day 2. At this early time point, differences in cell number and morphology were not yet readily discernible between SCN-iPS and control iPS cells, as shown in Fig. 2*A*. However, the microarray analysis revealed a differential expression of various genes between the two cell types. Transcription factor genes, which were related to neutrophil development [e.g., CCAAT/enhancer-binding protein (C/EBP)-α (20), C/EBP-β (21), C/EBP-ε (22), and SPI1 (also known as PU.1) (23)], were all down-regulated in SCN-iPS cells. B-cell chronic lymphocytic leukemia/lymphoma 2, which regulates cell death under ER stress through the core mitochondrial apoptosis pathway (24), was also down-regulated (Fig. 3*A*). These findings were confirmed by quantitative reverse-transcriptional PCR (qRT-PCR), as shown in Fig. 2*H*.

Notably, the down-regulation of the genes in SCN-iPS cells related to and regulated by the wingless-type mmtv integration site family, member 3a (Wnt3a)/β-catenin pathway [e.g., Wnt3a, lymphoid enhance-binding factor (LEF)-1, BIRC5 (also known as survivin), and cyclin D1] was also uncovered by microarray analysis and qRT-PCR (Fig. 3 *A–C* and Fig. S4). Therefore, we examined the effect of enhancement of Wnt3a/β-catenin signaling by exogenous Wnt3a addition on the neutrophil development of $CD34^+$ cells derived from SCN-iPS and control iPS cells. Although Wnt3a did not stimulate the survival, proliferation, and differentiation of $CD34^+$ cells derived from both iPS cells in the absence of cytokines stimulating myelopoiesis including G-CSF, the addition of Wnt3a to the neutrophil differentiation medium induced a dose-dependent increase in the percentage of mature neutrophils among the cultured cells, as shown in Fig. 3 *D* and *E*. Furthermore, when Wnt3a was added concurrently with 1,000ng/mL G-CSF, the proportion of mature neutrophils increased more than it did with Wnt3a or 1,000 ng/mL G-CSF alone, reaching a value comparable with that observed for control iPS cells (Fig. 4 *A* and *B*).

The reduced expression of LEF-1 (as regulated by the Wnt3a/β-catenin pathway) reportedly plays a critical role in the defective maturation of neutrophils in SCN patients (25). Therefore, we next examined LEF-1 mRNA expression in SCN-iPS–$CD34^+$ cells cultured in the presence of Wnt3a, G-CSF (1,000 ng/mL), or both. Wnt3a and G-CSF both enhanced LEF-1 mRNA expression, but the most significant increase was observed in the presence of Wnt3a plus G-CSF. LEF-1 expression in SCN-iPS–$CD34^+$ cells in response to Wnt3a plus G-CSF was almost the same as that in control iPS–$CD34^+$ cells (Fig. 4*C*). These results substantiate the importance of LEF-1 in neutrophil development and the pathogenesis of SCN, as shown (25). Moreover the

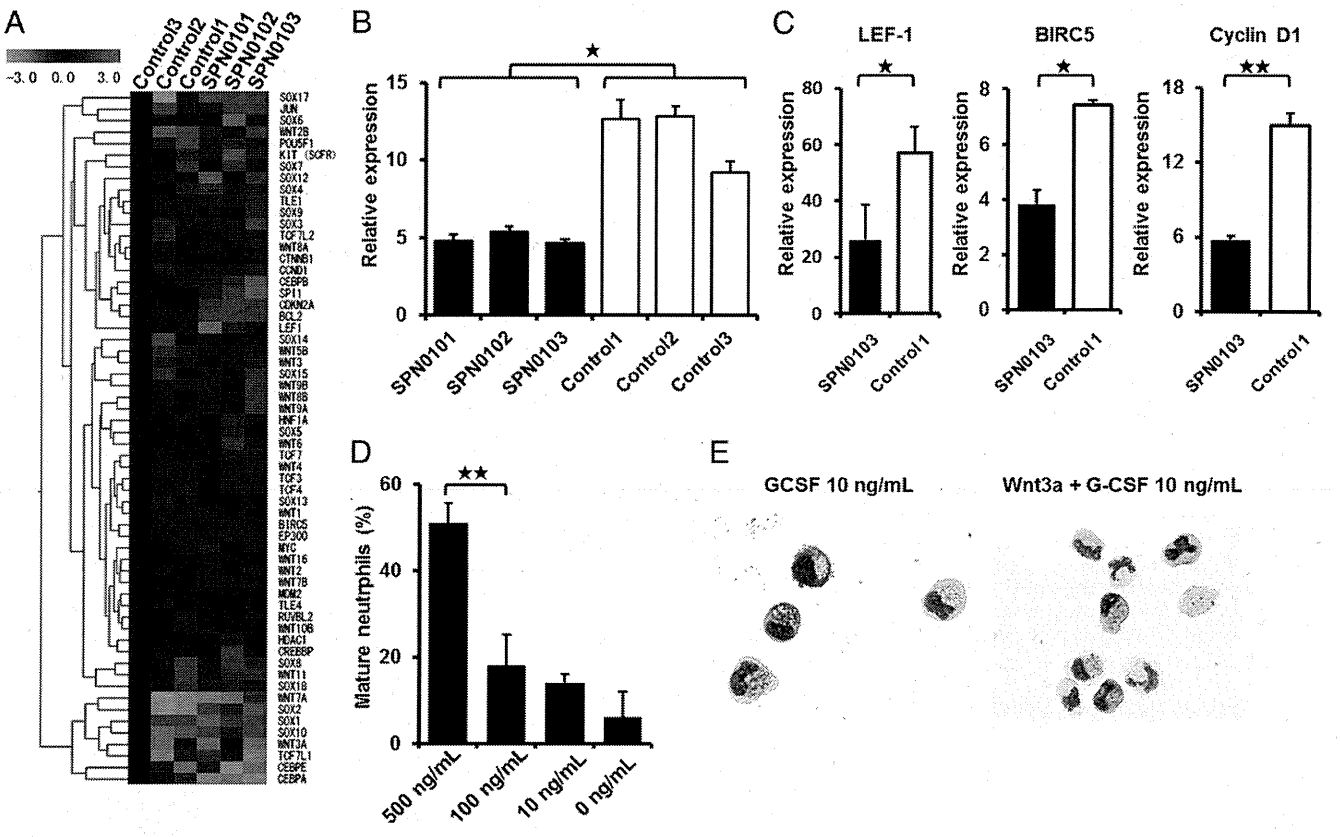

Fig. 3. Effects of Wnt3a on neutrophil development from SCN-iPS cells. (*A*) Heat map showing differential gene expression among SCN-iPS and control iPS cells on day 2. Red, high gene expression; blue, low gene expression compared with gene expression in control 3. (*B*) qRT-PCR analysis of the relative mRNA expression (target/HPRT expression) of Wnt3a on day 2. Filled and open bars indicate experiments using SCN-iPS cells (SPN0101, SPN0102, and SPN0103) and control iPS cells (controls 1, 2, and 3), respectively. Data are shown as mean ± SD. $^*P < 0.05$. (*C*) qRT-PCR analysis of the relative expression (target/HPRT expression) of genes regulated by the Wnt3a/β-catenin pathway (LEF-1, survivin, and cyclin D1) in SCN-iPS cells (filled bars, SPN0103) vs. control iPS cells (open bars, control 1) on day 2 of suspension culture. Data are shown as mean ± SD. $^{**}P < 0.01$; $^*P < 0.05$. (*D*) Proportion of mature neutrophils among the cells derived from SCN-iPS cells (SPN0102) on day 14 of suspension culture with dose escalation of Wnt3a. Data are shown as mean ± SD. $^{**}P < 0.01$. (*E*) Photographs of nonadherent cells on day 7 of suspension culture with or without Wnt3a (500 ng/mL) (400×; May–Grünwald–Giemsa staining).

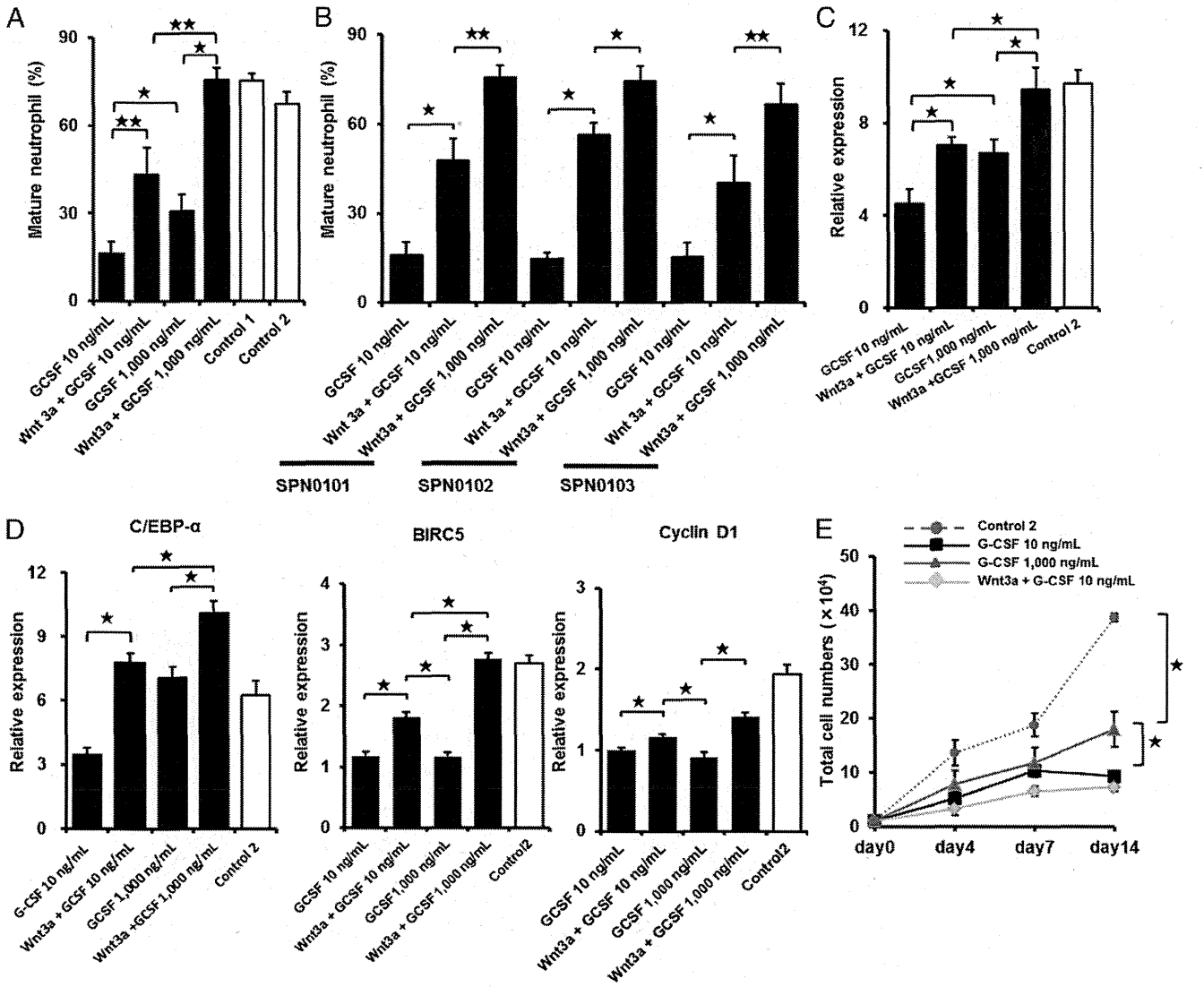

Fig. 4. Effects of Wnt3a in combination with high-dose G-CSF. (*A*) Filled and open bars show the proportion of mature neutrophils among the cells derived from SCN-iPS cells (SPN0101) on day 14 of suspension culture in the presence of neutrophil differentiation medium containing 10 ng/mL G-CSF (GCSF 10 ng/mL); 500 ng/mL Wnt3a and 10 ng/mL G-CSF (Wnt3a+GCSF 10 ng/mL); 1,000 ng/mL G-CSF (GCSF 1,000 ng/mL); or 500 ng/mL Wnt3a and 1,000 ng/mL G-CSF (Wnt3a + GCSF 1,000 ng/mL); and that from control iPS cells (controls 1 and 2) cultured in the neutrophil differentiation medium containing 10 ng/mL G-CSF, respectively. Data are shown as mean ± SD. $^{**}P < 0.01$; $^{*}P < 0.05$. (*B*) The proportion of mature neutrophils among the cells derived from three SCN-iPS cell clones (SPN0101, SPN0102, and SPN0103) on day 14 of suspension culture in the presence of neutrophil differentiation medium containing 10 ng/mL G-CSF (GCSF 10 ng/mL); 500 ng/mL Wnt3a and 10 ng/mL G-CSF (Wnt3a+GCSF 10 ng/mL); or 500 ng/mL Wnt3a and 1,000 ng/mL G-CSF (Wnt3a + GCSF 1,000 ng/mL). Data are shown as mean ± SD. $^{**}P < 0.01$; $^{*}P < 0.05$. (*C*) Filled and open bars show the relative expression (target/HPRT expression) of LEF-1 mRNA in SCN-iPS cells (SPN0101) on day 2 of suspension culture in the presence of differentiation medium containing the same combinations of Wnt3a and G-CSF as shown in *A* and that from control iPS cells (control 2), respectively. Data are shown as mean ± SD. $^{**}P < 0.01$; $^{*}P < 0.05$. (*D*) Filled and open bars show the relative expression (target/HPRT expression) of C/EBP-α, BIRC5, or cyclin D1 mRNA in SCN-iPS cells (SPN0101) on day 2 of suspension culture in the presence of differentiation medium containing the same combinations of Wnt3a and G-CSF as shown in *A* and that from control iPS cells (control 2), respectively. Data are shown as mean ± SD. $^{**}P < 0.01$; $^{*}P < 0.05$. (*E*) Total cell numbers of nonadherent cells in suspension cultures of 1×10^4 $CD34^+$ cells derived from control iPS cells (control 2; red broken line) and SCN-iPS cells (SPN0101) in the presence of neutrophil differentiation medium (black line) and those from SCN-iPS cells in the presence of neutrophil differentiation medium containing 500 ng/mL Wnt3a (yellow line) or 1,000 ng/mL G-CSF (black line). Data are shown as mean ± SD. $^{**}P < 0.05$.

administration of Wnt3a led to up-regulate C/EBP-α, cyclin D1, and BIRC5/survivin in addition to LEF-1 in the presence of G-CSF (Fig. 4*D*). These results suggested that the up-regulation of LEF-1 expression might promote granulopoiesis by increasing the expressions of cyclin D1, BIRC5/survivin, and C/EBP-α and its binding to LEF-1 in accordance with the previous report (25). Interestingly, Wnt3a did not stimulate the proliferation of myeloid cells, whereas 1,000 ng/mL G-CSF did to a certain extent (Fig. 4*E*). Hence, Wnt3a was capable of stimulating the maturation of impaired neutrophils in the presence of G-CSF, but not the proliferation of myeloid cells from SCN-iPS cells.

Importantly, aside from providing new insights into the mechanisms behind impaired neutrophil development in SCN patients, the present study demonstrates that agents activating the Wnt3a/β-catenin pathway are potential candidates for new drugs for SCN with mutations in the ELANE gene. Because endogenous G-CSF is readily increased in SCN patients (26), these activating agents may be viable alternatives to exogenous G-CSF treatment.

Materials and Methods

Additional information is available in *SI Materials and Methods*.

Generation of Human iPS Cells. BM fibroblasts from a patient with SCN and skin dermal fibroblasts from a healthy donor were acquired after obtaining informed consent after getting the approval by the Ethics Committee of the Institute of Medical Science, University of Tokyo, in accordance with the Declaration of Helsinki. The SCN patient presented with a heterozygous mutation in the ELANE gene in the 707 region of exon 5. SCN-iPS cells were established from the SCN-BM fibroblasts by transfection with the pMX retroviral vector, as described (10). This vector expressed the human transcription factors OCT3/4, SOX2, KLF4, and c-MYC. Control iPS cell clones, control 1 (TkDN4-M) and control 3 (201B7), were gifts from K. Eto and S. Yamanaka (Kyoto University, Kyoto), respectively (10, 11). Control 2 (SPH0101) was newly generated from another healthy donor's skin dermal fibroblasts by using the same methods.

Hematopoietic Colony Assay. A hematopoietic colony assay was performed in an aliquot of culture mixture, which contained 1.2% methylcellulose (Shin-Etsu Chemical), 30% (vol/vol) FBS, 1% (vol/vol) deionized fraction V BSA, 0.1 mM 2-mercaptoethanol (2-ME), α-minimum essential medium, and a cytokine mixture consisting of 100 ng/mL human stem cell factor (hSCF) (Wako), 100 ng/mL fusion protein 6 [FP6; a fusion protein of interleukin (IL)-6 and IL-6 receptor] (a gift from Tosoh), 10 ng/mL human IL-3 (hIL-3) (a gift from Kirin Brewery), 10 ng/mL human thrombopoietin (hTPO) (a gift from Kirin Brewery), 10 ng/mL human G-CSF (a gift from Chugai Pharmaceutical), and 5 U/mL human erythropoietin (a gift from Kirin Brewery). For dose escalation experiments, various concentrations (0, 1, 10, 100, and 1,000 ng/mL) of G-CSF were used instead of the cytokine mixture described above. Colony types were determined according to established criteria on day 14 of culture by in situ observations under an inverted microscope (IX70; Olympus) (27).

Suspension Culture and Neutrophil Differentiation Assay. $CD34^+$ cells (1×10^4 cells) were cocultured with irradiate confluent AGM-S3 cells in neutrophil differentiation medium containing Iscove's modified Dulbecco's medium, 10% FBS, 3 mM L-glutamine, 1×10^{-4} M 2-ME, 1×10^{-4} M nonessential amino acids solution, 100 ng/mL hSCF, 100 ng/mL FP6, 10 ng/mL hIL-3, 10 ng/mL hTPO, and 10 or 1,000 ng/mL human G-CSF. Wnt3a (10, 100, or 500 ng/mL) (R&D) was then added. The medium was replaced with an equivalent volume of fresh medium every 4 d. Living, nonadherent cells were counted following 0.4% trypan blue staining.

PCR primer. All primer sets used in this study are shown in Table S1.

Statistical Analysis. All data are presented as mean ± SD. $P < 0.05$ was considered significant. Statistical analyses were performed by using Prism software (GraphPad).

ACKNOWLEDGMENTS. We thank the individual with SCN who participated in this study; K. Eto for providing control iPS cells (control 1; TkDN4-M); S. Yamanaka for providing control iPS cells (control 3; 206B7); and E. Matsuzaka and S. Hanada for technical assistance. This work was supported by in part by Ministry of Education, Culture, Sports, Science, and Technology of Japan (MEXT) Grants-in-Aid (to Y.E.) and Project for Realization of Regenerative Medicine (MEXT) Grants-in-Aid (to K.Tsuji).

1. Zeidler C, Germeshausen M, Klein C, Welte K (2009) Clinical implications of *ELA2-, HAX1-*, and G-CSF-receptor (*CSF3R*) mutations in severe congenital neutropenia. *Br J Haematol* 144(4):459–467.
2. Freedman MH, et al. (2000) Myelodysplasia syndrome and acute myeloid leukemia in patients with congenital neutropenia receiving G-CSF therapy. *Blood* 96(2):429–436.
3. Dale DC, et al. (1993) A randomized controlled phase III trial of recombinant human granulocyte colony-stimulating factor (filgrastim) for treatment of severe chronic neutropenia. *Blood* 81(10):2496–2502.
4. Rosenberg PS, et al.; Severe Chronic Neutropenia International Registry (2006) The incidence of leukemia and mortality from sepsis in patients with severe congenital neutropenia receiving long-term G-CSF therapy. *Blood* 107(12):4628–4635.
5. Xia J, et al. (2009) Prevalence of mutations in ELANE, GFI1, HAX1, SBDS, WAS and G6PC3 in patients with severe congenital neutropenia. *Br J Haematol* 147(4):535–542.
6. Horwitz MS, et al. (2007) Neutrophil elastase in cyclic and severe congenital neutropenia. *Blood* 109(5):1817–1824.
7. Hajjar E, Broemstrup T, Kantari C, Witko-Sarsat V, Reuter N (2010) Structures of human proteinase 3 and neutrophil elastase—so similar yet so different. *FEBS J* 277(10): 2238–2254.
8. Fouret P, et al. (1989) Expression of the neutrophil elastase gene during human bone marrow cell differentiation. *J Exp Med* 169(3):833–845.
9. Pham CT (2006) Neutrophil serine proteases: Specific regulators of inflammation. *Nat Rev Immunol* 6(7):541–550.
10. Takayama N, et al. (2010) Transient activation of c-MYC expression is critical for efficient platelet generation from human induced pluripotent stem cells. *J Exp Med* 207(13):2817–2830.
11. Takahashi K, et al. (2007) Induction of pluripotent stem cells from adult human fibroblasts by defined factors. *Cell* 131(5):861–872.
12. Germeshausen M, Ballmaier M, Welte K (2007) Incidence of CSF3R mutations in severe congenital neutropenia and relevance for leukemogenesis: Results of a long-term survey. *Blood* 109(1):93–99.
13. Ma F, et al. (2007) Novel method for efficient production of multipotential hematopoietic progenitors from human embryonic stem cells. *Int J Hematol* 85(5):371–379.
14. Konishi N, et al. (1999) Defective proliferation of primitive myeloid progenitor cells in patients with severe congenital neutropenia. *Blood* 94(12):4077–4083.
15. Nakamura K, et al. (2000) Abnormalities of primitive myeloid progenitor cells expressing granulocyte colony-stimulating factor receptor in patients with severe congenital neutropenia. *Blood* 96(13):4366–4369.
16. Skokowa J, Fobiwe JP, Dan L, Thakur BK, Welte K (2009) Neutrophil elastase is severely down-regulated in severe congenital neutropenia independent of ELA2 or HAX1 mutations but dependent on LEF-1. *Blood* 114(14):3044–3051.
17. Kawaguchi H, et al. (2003) Dysregulation of transcriptions in primary granule constituents during myeloid proliferation and differentiation in patients with severe congenital neutropenia. *J Leukoc Biol* 73(2):225–234.
18. Köllner I, et al. (2006) Mutations in neutrophil elastase causing congenital neutropenia lead to cytoplasmic protein accumulation and induction of the unfolded protein response. *Blood* 108(2):493–500.
19. Grenda DS, et al. (2007) Mutations of the ELA2 gene found in patients with severe congenital neutropenia induce the unfolded protein response and cellular apoptosis. *Blood* 110(13):4179–4187.
20. Pabst T, et al. (2001) AML1-ETO downregulates the granulocytic differentiation factor C/EBPalpha in t(8;21) myeloid leukemia. *Nat Med* 7(4):444–451.
21. Hirai H, et al. (2006) C/EBPbeta is required for 'emergency' granulopoiesis. *Nat Immunol* 7(7):732–739.
22. Bedi R, Du J, Sharma AK, Gomes I, Ackerman SJ (2009) Human C/EBP-ε activator and repressor isoforms differentially reprogram myeloid lineage commitment and differentiation. *Blood* 113(2):317–327.
23. Friedman AD (2007) Transcriptional control of granulocyte and monocyte development. *Oncogene* 26(47):6816–6828.
24. Hetz C (2012) The unfolded protein response: Controlling cell fate decisions under ER stress and beyond. *Nat Rev Mol Cell Biol* 13(2):89–102.
25. Skokowa J, et al. (2006) LEF-1 is crucial for neutrophil granulocytopoiesis and its expression is severely reduced in congenital neutropenia. *Nat Med* 12(10):1191–1197.
26. Mempel K, Pietsch T, Menzel T, Zeidler C, Welte K (1991) Increased serum levels of granulocyte colony-stimulating factor in patients with severe congenital neutropenia. *Blood* 77(9):1919–1922.
27. Nakahata T, Ogawa M (1982) Hemopoietic colony-forming cells in umbilical cord blood with extensive capability to generate mono- and multipotential hemopoietic progenitors. *J Clin Invest* 70(6):1324–1328.

blood

2012 119: 5458-5466
Prepublished online April 19, 2012;
doi:10.1182/blood-2011-05-354167

Frequent somatic mosaicism of *NEMO* in T cells of patients with X-linked anhidrotic ectodermal dysplasia with immunodeficiency

Tomoki Kawai, Ryuta Nishikomori, Kazushi Izawa, Yuuki Murata, Naoko Tanaka, Hidemasa Sakai, Megumu Saito, Takahiro Yasumi, Yuki Takaoka, Tatsutoshi Nakahata, Tomoyuki Mizukami, Hiroyuki Nunoi, Yuki Kiyohara, Atsushi Yoden, Takuji Murata, Shinya Sasaki, Etsuro Ito, Hiroshi Akutagawa, Toshinao Kawai, Chihaya Imai, Satoshi Okada, Masao Kobayashi and Toshio Heike

Blood (print ISSN 0006-4971, online ISSN 1528-0020), is published weekly by the American Society of Hematology, 2021 L St, NW, Suite 900, Washington DC 20036.

Frequent somatic mosaicism of *NEMO* in T cells of patients with X-linked anhidrotic ectodermal dysplasia with immunodeficiency

Tomoki Kawai,[1] Ryuta Nishikomori,[1] Kazushi Izawa,[1] Yuuki Murata,[1] Naoko Tanaka,[1] Hidemasa Sakai,[1] Megumu Saito,[2] Takahiro Yasumi,[1] Yuki Takaoka,[1] Tatsutoshi Nakahata,[2] Tomoyuki Mizukami,[3] Hiroyuki Nunoi,[3] Yuki Kiyohara,[4] Atsushi Yoden,[5] Takuji Murata,[5] Shinya Sasaki,[6] Etsuro Ito,[6] Hiroshi Akutagawa,[7] Toshinao Kawai,[8] Chihaya Imai,[9] Satoshi Okada,[10] Masao Kobayashi,[10] and Toshio Heike[1]

[1]Department of Pediatrics, Kyoto University Graduate School of Medicine, Kyoto, Japan; [2]Clinical Application Department, Center for iPS Cell Research and Application, Institute for Integrated Cell-Material Sciences, Kyoto University, Kyoto, Japan; [3]Division of Pediatrics, Department of Reproductive and Developmental Medicine, Faculty of Medicine, University of Miyazaki, Miyazaki, Japan; [4]Department of Pediatrics, Faculty of Medicine, Osaka University, Suita, Japan; [5]Department of Pediatrics, Osaka Medical College, Takatsuki, Japan; [6]Department of Pediatrics, Hirosaki University Graduate School of Medicine, Hirosaki, Japan; [7]Department of Pediatrics, Kishiwada City Hospital, Kishiwada, Japan; [8]Department of Human Genetics, National Center for Child Health and Development, Tokyo, Japan; [9]Department of Pediatrics, Niigata University, Niigata, Japan; and [10]Department of Pediatrics, Hiroshima University Graduate School of Biomedical Sciences, Hiroshima, Japan

Somatic mosaicism has been described in several primary immunodeficiency diseases and causes modified phenotypes in affected patients. X-linked anhidrotic ectodermal dysplasia with immunodeficiency (XL-EDA-ID) is caused by hypomorphic mutations in the *NF-κB essential modulator (NEMO)* gene and manifests clinically in various ways. We have previously reported a case of XL-EDA-ID with somatic mosaicism caused by a duplication mutation of the *NEMO* gene, but the frequency of somatic mosaicism of *NEMO* and its clinical impact on XL-EDA-ID is not fully understood. In this study, somatic mosaicism of *NEMO* was evaluated in XL-EDA-ID patients in Japan. Cells expressing wild-type NEMO, most of which were derived from the T-cell lineage, were detected in 9 of 10 XL-EDA-ID patients. These data indicate that the frequency of somatic mosaicism of *NEMO* is high in XL-ED-ID patients and that the presence of somatic mosaicism of *NEMO* could have an impact on the diagnosis and treatment of XL-ED-ID patients. (*Blood.* 2012;119(23):5458-5466)

Introduction

X-linked anhidrotic ectodermal dysplasia with immunodeficiency (XL-EDA-ID) is a disease with clinical features including hypohidrosis, delayed eruption of teeth, coarse hair, and immunodeficiency associated with frequent bacterial infections.[1-5] The gene responsible for XL-EDA-ID has been identified as *NF-κB essential modulator (NEMO)*.[6-8] NEMO is necessary for the function of IκB kinase, which phosphorylates and degrades IκB to activate NF-κB.[9-10] Defects in NEMO cause various abnormalities in signal transduction pathways involving NF-κB, and affect factors such as the IL-1 family protein receptors, the TLRs, VEGFR-3, receptor activator of nuclear factor κB (RANK), the ectodysplasin-A receptor, CD40, and the TNF receptor I.[7] Whereas a complete loss of NEMO function in humans is believed to cause embryonic lethality,[11] *NEMO* mutations in XL-EDA-ID patients are hypomorphic,[8] causing a partial loss of NEMO functions.

In XL-EDA-ID, NEMO defects lead to diverse immunologic features including susceptibility to pathogens, impaired Ab response to polysaccharides,[2,4,12] hypogammaglobulinemia,[13] hyper IgM syndrome,[14] and impaired NK-cell activity,[15] with a large degree of variability in phenotypes among the patients. For example, approximately one-tenth of XL-EDA-ID patients exhibit reduced mitogen-induced proliferation of T lymphocytes.[12] Moreover, one-fourth suffer from inflammatory disorders such as inflammatory bowel disease and rheumatoid arthritis,[12] although the inflammatory process usually relies on NF-κB activation.[16] One explanation for this clinical variability is that the XL-EDA-ID phenotype is *NEMO* genotype-specific. Although the XL-EDA-ID database reported by Hanson et al succeeds to some extent in linking the specific clinical features to *NEMO* genotype,[12] the penetrance of some clinical features is not high and the mechanism accounting for this variability is unknown.

Recently, we have reported a case of spontaneous reversion mosaicism of the *NEMO* gene in XL-EDA-ID, which showed an atypical phenotype involving decreased mitogen-induced T-cell proliferation along with decreased CD4 T cells (patient 1).[17] There have been no subsequent reports on somatic mosaicism in XL-EDA-ID, and its prevalence and impact on the clinical features of the disease is unknown. In this study, we describe the younger brother of patient 1, who suffered from XL-EDA-ID with the same mutation and somatic reversion mosaicism of *NEMO*. Patient 2 showed intriguing laboratory findings in that mitogen-induced T-cell proliferation varied in accordance with the rate of detected reversion in the peripheral blood. These 2 cases led us to perform a nationwide study of XL-EDA-ID patients in Japan that revealed a high incidence of somatic mosaicism of *NEMO*.

Submitted May 11, 2011; accepted April 8, 2012. Prepublished online as *Blood* First Edition paper, April 19, 2012; DOI 10.1182/blood-2011-05-354167.

The online version of this article contains a data supplement.

The publication costs of this article were defrayed in part by page charge payment. Therefore, and solely to indicate this fact, this article is hereby marked "advertisement" in accordance with 18 USC section 1734.

Table 1. Clinical and genetic features of XL-EDA-ID patients

Patient	Mutation	Ectodermal dysplasia	Mitogen-induced proliferation	Infections	Complications	Therapy	Sex chromosome chimerism
1	Duplication	+	Reduced	Sepsis (S.P. and P.A.)	Chronic diarrhea	IVIG	100% XY
				Disseminated M.A.C.	Failure to thrive	RFP, CAM, AMK, EB	
				Skin abscess (S.A.)	Small intestinal stenosis	Rifabutin	
				Invasive *Aspergillus*	Lymphedema		
2	Duplication	+	Reduced	Sepsis (*E coli*)	Failure to thrive	IVIG, ST, EB, CAM	99.8% XY 0.2% X
				Disseminated M.S.		Rifabutin, SCT	
3	D311E	−	Normal	Disseminated B.C.G.		IVIG, INH	100% XY
				Sepsis (S.P.)		RFP, SCT	
4	A169P	+	Normal	Meningitis (S.P.)	IBD	IVIG, ST, PSL	99% XY
					Interstitial pneumonia	CyA, MTX, Infliximab	
					Rheumatoid arthritis		
5	L227P	+	Normal	Recurrent pneumonia	IBD	ST, mesalazine	Not done
				Pyogenic coxitis		Infliximab	
				Recurrent otitis media			
6	R182P	+	Not done	Recurrent otitis media	IBD	ST, mesalazine	99.8% XY 0.2% X
				UTI, Recurrent stomatitis			
				Subepidermal abscess			
7	R175P	+	Normal	Recurrent sepsis (S.P.)		IVIG	100% XY
8	Q348X	+	Normal	Disseminated B.C.G.	IBD	IVIG, ST	100% XY
9	R175P	+	Normal	Recurrent pneumonia	IBD	IVIG	100% XY
				Recurrent otitis media		5-aminosalicylic acid	
				Kaposi varicelliform eruption			
10	1167 ins C	+	Normal	Sepsis and Enteritis (E.A)	Failure to thrive	IVIG, SCT	Not done
				Sepsis (C.G.)	Pyloric stenosis, colon polyps		
				UTI (K.P.)			

S.P. indicates *Streptococcus pneumoniae*; P.A., *Pseudomonas aeruginosa*; IVIG, intravascular immunoglobulin infusion; M.A.C., *Mycobacterium avium* complex; S.A., *Staphylococcus aureus*; *E coli*, *Escherichia coli*; ST, trimethoprim-sulfamethoxazole; M.S., *Mycobacterium szulgai*; AMK, amikacin; EB, ethambutol; CAM, clarithromycin; SCT, stem cell transplantation; B.C.G., Bacille de Calmette et Guerin; INH, isoniazid; RFP, rifampicin; IBD, inflammatory bowel disease; PSL, prednisolone; CyA, cyclosporine A; MTX, methotrexate; UTI, urinary tract infection; E.A., *Enterobacter aerogenes*; C.G., *Candida glabrata*; and K.P., *Klebsiella* pneumonia.

Methods

Informed consent

Informed consent was obtained from the patients and their families following the Declaration of Helsinki according to the protocol of the Internal Review Board of Kyoto University, which approved this study.

Patients

Patient 1 was an XL-EDA-ID patient with a duplication mutation of the *NEMO* gene spanning intron 3 to exon 6. This patient has been reported previously[17] and died from an *Aspergillus* infection at the age of 4. Patient 2, born at term, was the younger brother of patient 1. This patient was also diagnosed as XL-EDA-ID with the same duplication mutation as patient 1 by genetic study. He received trimethoprim-sulfamethoxazole prophylaxis and a monthly infusion of immunoglobulin from the age of 1 month. The patient maintained good health and had a body weight of 7899*g* at 6 months when he started to fail to thrive. Except for poor weight gain, patient 2 appeared active with a good appetite, negative C-reactive protein, normal white blood cell counts, and no apparent symptoms. At 19 months of age, *Mycobacterium szulgai* was detected by venous blood culture, and the patient was treated with multidrug regimens including ethambutol, rifabutin, and clarithromycin based on the treatment of systemic *Mycobacterium avium* complex infection. The patient responded well to the treatment and his weight increased from 7830*g* to 9165*g* within a month after the treatment was initiated. Patient 2 received an unrelated cord blood cell transplantation at 26 months of age, containing 8.5×10^7 nucleated cells/kg (4.4×10^5 $CD34^+$ cells/kg), which was matched at 5 of 8 loci: mismatches occurred at 1 HLA-B and 1 HLA-C allele (according to serology), and at 1 HLA-A, 1 HLA-B, and 1 HLA-C allele (according to DNA typing). The preconditioning regimen consisted of fludarabine (30 mg/m^2/d) on days −7 to −3, melphalan (70 mg/m^2/d) on days −6 to −5, and rabbit anti-thymocyte globulin (2.5 mg/kg/d) on days −6 to −2. At first, Tacrolimus (0.024 mg/kg/d) was used to prevent GVHD, but this was switched to cyclosporin A (3 mg/kg/d) on day 9 because of drug-induced encephalopathy. Neutrophil ($> 0.5 \times 10^9$/L) and platelet ($> 50 \times 10^9$/L) engraftment were examined on days 13 and 40, respectively. Although $CD19^+$ cells (2042/μL, 94% donor chimerism), $CD56^+$ cells (242/μL, 97% donor chimerism), and monocytes (557/μL, 69% donor chimerism) were successfully generated, $CD3^+$ cells were not detected in the peripheral blood by day 54. The patient suffered from septic shock and died on day 60. Patients 3 to 10 were XL-EDA-ID patients recruited nationwide in Japan. Clinical details of patients 3, 4, and 10 have been reported previously.[18-20] These patients had clinical phenotypes characteristic of XL-EDA-ID such as ectodermal dysplasia, innate and/or acquired immunity defects, and susceptibility to pyogenic bacteria and *Mycobacterium* infection. Every patient had a mutation in the *NEMO* gene that caused reduced NF-κB activation in a NEMO reconstitution assay, as described in "Proliferation of $NEMO^{normal}$ and $NEMO^{low}$ T cells." Patient profiles are listed in Table 1.

Flow cytometric analysis

NEMO intracellular staining was performed as previously described.[17] The cells were stained for the following lineage markers before staining for NEMO: CD4, CD8, CD14, CD15, CD19, CD56, CD45RA (BD Biosciences/BD Pharmingen), and CCR7 (R&D Systems Inc). Intracellular staining of human IFN-γ, TNF-α, and NEMO was performed as previously described.[18] The stained cells were collected using a FACSCalibur flow cytometer (BD Biosciences) and analyzed using the FlowJo software (TreeStar).

Reporter assay

Wild-type and mutant *NEMO* cDNAs were generated from a healthy volunteer and the recruited XL-EDA-ID patients by RT-PCR; the cDNAs were subcloned into the p3xFLAG-CMV14 vector (Sigma-Aldrich). NEMO null rat fibroblast cells (kindly provided by Dr S. Yamaoka, Department of Molecular Virology, Graduate School of Medicine, Tokyo Medical and Dental University, Tokyo, Japan) were plated at a density of

3×10^4 cells/well in a 24-well culture dish and were transfected with 40 ng of NF-κB reporter plasmid (pNF-κB-Luc; BD Biosciences/BD Clontech), 2 ng of *NEMO* mutant expression construct, 10 ng of internal control for the normalization of transfection efficiency (pRL-TK; Toyo Ink), and 148 ng of mock vector using FuGENE HD Transfection Reagent (TOYO-B-Net) according to the manufacturer's protocol. Twelve hours after transfection, the cells were stimulated with 15 ng/mL lipopolysaccharide (LPS; Sigma-Aldrich) for 4 hours and the NF-κB activity was measured using the PicaGene Dual SeaPansy assay kit (TOYO-B-Net). Experiments were performed in triplicate and firefly luciferase activity was normalized to *Renilla* luciferase activity.

Subcloning analysis of cDNA

Cell sorting of the various cell lineages was performed by FACSVantage (BD Biosciences). The purity of each lineage was > 95%. The cDNA from sorted cells was purified and reverse transcribed by Super Script III (Invitrogen) with random hexamers and amplified by the proofreading PCR enzyme KOD, as previously described.[17,21] The PCR primers used were NEMO2 (5′-AGAGACGAAGGAGCACAAAGCTGCCTTGAG-3′) and NEMO3 (5′-ACTGCAGGGACAATGGTGGGTGCATCTGTC-3′). The PCR products were subcloned using a TA cloning kit (Invitrogen) and sequenced by ABI 3130xl Genetic analyzer (Applied Biosystems). To determine whether additional mutations occurred in revertant subclones that had wild-type sequence in the original mutation site, the entire coding region of the *NEMO* gene was sequenced and an additional mutation was considered present when the same mutation was detected in multiple subclones.

Allele-specific PCR

The mRNA purified from sorted T cells and monocytes was reverse-transcribed by SuperScript III (Invitrogen) with the gene-specific primer NEMO2 and amplified by the proofreading PCR enzyme KOD (Toyobo) using the primers NEMO3 and NEMO 4 (5′-TGTGGACACGCAGTGAAACGTGGTCTGGAG-3′). The PCR products were used as templates for allele-specific PCRs with Ex Taq polymerase (Takara Bio). Mutant and wild-type *NEMO* DNA was generated from each NEMO expression plasmid, mixed at graded ratios, and used as controls. PCR conditions and primer sequences are listed in supplemental Table 1 (available on the *Blood* Web site; see the Supplemental Materials link at the top of the online article).

Proliferation of NEMO^{normal} and NEMO^{low} T cells

To obtain PHA-induced T-cell blasts, PBMCs were stimulated with PHA (1:100; Invitrogen) and cultured in RPMI 1640 supplemented with 5% FCS and recombinant human IL-2 (50 IU/mL; kindly provided by Takeda Pharmaceutical Company) at 37°C for 7 days. Subcloning analysis of the cDNA obtained from the T-cell blasts was performed as described in "Subcloning analysis of cDNA."

Results

Reversion mosaicism of NEMO occurred in siblings with similar immunologic phenotypes

We previously reported patient 1 with a duplication mutation of the *NEMO* gene spanning intron 3 to exon 6, who was diagnosed as XL-EDA-ID at 1 year of age after suffering from recurrent infections.[17] At first, genetic diagnosis of the patient was difficult because the expression of aberrant *NEMO* mRNA was masked by the expression of normal *NEMO* mRNA by the revertant cells. Flow cytometric analysis of intracellular NEMO expression revealed cells with normal (NEMO^{normal}) and reduced (NEMO^{low}) levels of NEMO expression, indicating the presence of reversion mosaicism of the *NEMO* gene, and further analysis revealed that the *NEMO* mutation was disease-causing. PCR across the mutated region and sequencing of the PCR products revealed a duplication extending from intron 3 to exon 6, which was confirmed by Southern blot analysis. Additional copy number analysis of the *NEMO* gene of patient 1 and his mother excluded the possibility of a complex chromosomal aberration such as multiple duplication of the *NEMO* gene (supplemental Figure 1). Furthermore, polymorphism analysis using variable number tandem repeats on NEMO^{normal} and NEMO^{low} cells from patient 1 revealed that these cells were derived from the same origin (supplemental Table 2), indicating that the *NEMO* gene mosaicism was less likely because of amalgamation. The genomic analysis of the NEMO^{normal} cells revealed a complete reversion of the *NEMO* gene with no additional mutations. The clinical phenotype of patient 1 was combined immunodeficiency with a reduced number of T cells and mitogen-induced proliferation (Tables 2-3). We previously determined that reduced NEMO expression in the mutant T cells caused impairment of T-cell development and mitogen-induced proliferation.

Patient 2, the younger brother of patient 1, was diagnosed as XL-EDA-ID with the same duplication mutation as his brother. Flow cytometric analysis of intracellular NEMO expression performed at diagnosis showed that most of his PBMCs had reduced NEMO expression (Figure 1A). At 2 months of age, when most of the T cells were NEMO^{low}, absolute counts of the patient's T cells and the mitogen-induced proliferation of the patient's PBMCs were comparable with those of the healthy controls (Figure 1A-B; Table 2). These findings indicated that the *NEMO* mutation had no effect on T-cell development and mitogen-induced proliferation during early infancy in patient 2.

NEMO^{normal} T cells gradually increased as patient 2 grew older, while the absolute count of NEMO^{low} T cells decreased (Figure 1A-B). Accordingly, normal full-length *NEMO* cDNA, which had been undetectable in cord blood, was detectable in the patient's peripheral blood at 12 months of age. However, while NEMO^{normal} T cells were increasing, mitogen-induced T-cell proliferation started to decrease (Table 3), and the patient started to show poor weight gain from 6 months of age. When patient 2 was 17 months old, a blood culture revealed an *M szulgai* bacteremia. At this time, the absolute count of NEMO^{normal} T cells peaked, and NEMO^{low} T cells were at a minimum. He began to gain weight after anti-*Mycobacterium* medication was initiated, although NEMO^{normal} T cells started to decrease and NEMO^{low} T cells began to increase (Figure 1B). When the patient was 23 months old, mitogen-induced T-cell proliferation was still low and a roughly equal number of NEMO^{low} and NEMO^{normal} T cells were detected (Table 3). Overall, as patient 2 grew older, NEMO^{normal} T cells increased as the total number of T cells and the mitogen-induced T-cell proliferation decreased, similar to what had occurred in patient 1 at a similar age.

Various analyses were performed to compare the immunologic phenotype of NEMO^{low} and NEMO^{normal} T cells in detail. Both NEMO^{normal} and NEMO^{low} CD4$^+$ T cells carried a diverse Vβ repertoire, but CD8$^+$ T cells had a skewed Vβ repertoire regardless of NEMO expression level (Figure 1C). Surface marker analysis revealed that most of the NEMO^{normal} T cells were CD45RA$^-$/CCR7$^-$ and most of the NEMO^{low} T cells were CD45RA$^+$/CCR7$^+$ (Figure 1D). The NEMO^{normal} T cells produced similar amounts of IFN-γ and TNF-α as healthy control cells, while the production of these cytokines were reduced in NEMO^{low} T cells (Figure 1E-F). Taken together, these data implied that the immunologic phenotype of T cells from patient 2 converged with that of patient 1 as patient 2 grew older.

Table 2. Surface marker analysis of peripheral mononuclear cells of patients 1 and 2

	Patient 1	Patient 2		Healthy controls
Age at analysis	2 y	2 mo	19 mo	
CD3	1503	2366	1014	2997 ± 1751
CD4	292	1583	374	1683 ± 874
CD8	1160	783	547	1114 ± 976
TCRαβ	1386	2295	439	2620 ± 1612
TCRγδ	109	74	574	343 ± 177
$CD4^+CD45RA$	58	1336	105	1471 ± 890
$CD4^+CD45RO$	263	307	266	497 ± 189
$CD8^+CD45RA$	1178	783	297	1083 ± 1078
$CD8^+CD45RO$	361	21	250	385 ± 442
$CD4^+CD25$	80	427	93	210 ± 99
CD19	1200	941	1543	1252 ± 1145
CD20	1189	931	1536	1125 ± 837
$CD19^+$Sm-IgG	7	18	17	54 ± 21
$CD19^+$Sm-IgA	15	4	14	18 ± 14
$CD19^+$Sm-IgM	1171	910	1505	1057 ± 881
$CD19^+$Sm-IgD	1171	906	1495	1052 ± 884
CD16	912	176	24	287 ± 200
CD56	908	176	24	306 ± 207

Surface markers expressed by XL-EDA-ID patients' PBMCs are shown as absolute counts per microliter of peripheral blood. Healthy control values are based on children aged 1 to 6 years and are shown as the mean ± SD.

Sm indicates the surface membrane.

High incidence of somatic mosaicism of the *NEMO* gene in XL-EDA-ID patients

It is worth noting that somatic reversion mosaicism of the *NEMO* gene occurred in both of the 2 XL-EDA-ID siblings carrying a duplication mutation. To determine whether a high frequency of reversion is a specific event for this type of *NEMO* duplication mutation[22-25] or if the reversion of the *NEMO* gene occurs commonly in XL-EDA-ID patients, we recruited an additional 8 XL-EDA-ID patients from throughout Japan (Table 1) and analyzed the presence of *NEMO* reversion. These patients had various combinations of clinical phenotypes characteristic of XL-EDA-ID such as ectodermal dysplasia, innate and acquired immunity defects, and susceptibility to pyogenic bacteria and *Mycobacterium* infections. Every patient had a mutation of the *NEMO* gene with reduced NF-κB activation potential, as evaluated in a NEMO reconstitution assay (Figure 2).

Among the 8 patients, only patient 3 had a large proportion of $NEMO^{low}$ cells by flow cytometric analysis. The majority of patient 3's PBMCs were $NEMO^{low}$, whereas 10% of the patient's $CD8^+$ cells were $NEMO^{normal}$ (Figure 3A). This patient was identified as carrying the D311E mutation. Because missense mutations of the *NEMO* gene often do not result in the reduced expression of NEMO protein, subcloning and sequencing analysis was performed on the *NEMO* cDNA isolated from the remaining patients, and 6 of the 7 patients had normal *NEMO* subclones (Table 3). Expansion of maternal cells after fetomaternal transfusion was ruled out in these patients by FISH analysis with X and Y probes (Table 1).

Additional genetic analysis of the entire coding region of the *NEMO* gene was performed on $NEMO^{normal}$ cells from patient 3 and on reverted subclones from the other patients, except for patient 10 who had already received stem cell transplantation. The *NEMO* gene in these samples had reverted to wild-type with no additional mutations (Figure 3B and data not shown). To specifically determine in which cell lineages the reversion occurred, subcloning and sequencing analysis of cDNA in various cell lineages was performed. This analysis revealed that all the revertant cells were of the T-cell lineage and that no reversion occurred in monocytes and very little occurred in B cells (Table 4). Allele-specific PCR confirmed that reversion occurred in T cells but not in monocytes (Figure 4).

Selective advantage of $NEMO^{normal}$ cells in XL-EDA-ID carriers

The high frequency of somatic mosaicism in T cells of XL-EDA-ID patients indicated a strong selective advantage of wild-type NEMO T cells over T cells carrying mutant NEMO. To confirm this hypothesis, *NEMO* cDNA analysis was performed on various cell lineages from the mothers of the patients who are heterozygous for *NEMO* mutation and thus have mosaicism

Table 3. Immunologic analysis of patients 1 and 2

	Patient 1	Patient 2 (treated with IVIG)	
Age at analysis, mo	9	9	20
Serum immunoglobulin levels, g/L (control)			
IgG	10.63 (4.51-10.46)	8.44 (4.51-10.46)	10.37 (7.15-9.07)
IgA	1.36 (0.14-0.64)	1.88 (0.14-0.64)	3.93 (0.22-1.44)
IgM	0.4 (0.33-1.00)	0.17 (0.33-1.00)	0.20 (0.34-1.28)
Age at analysis	2 y	2 mo	23 mo
T-cell proliferation, SI (control)	9.3 (206.9 ± 142.5)	55.3 (64.8 ± 8.1)	7.2 (89.4 ± 31.2)

Control values of serum immunoglobulin levels are based on children aged either 7 to 9 months or 1 to 2 years and are shown as the mean ± SD. The T-cell proliferation assay was performed as described previously[17] with at least three healthy adults as controls.

SI indicates stimulation index; and IVIG, 2.5 g of monthly IV immune globulin infusion.